



HAL
open science

Call for participation: Collaborative benchmarking of functional-structural root architecture models. The case of root water uptake

Andrea Schnepf, Christopher K Black, Valentin Couvreur, Benjamin M Delory, Claude Doussan, Axelle Koch, Timo Koch, Mathieu Javaux, Magdalena Landl, Daniel Leitner, et al.

► **To cite this version:**

Andrea Schnepf, Christopher K Black, Valentin Couvreur, Benjamin M Delory, Claude Doussan, et al.. Call for participation: Collaborative benchmarking of functional-structural root architecture models. The case of root water uptake. 2019. <hal-04210395>

HAL Id: hal-04210395

<https://hal.science/hal-04210395v1>

Preprint submitted on 18 Sep 2023

HAL is a multi-disciplinary open access archive for the deposit and dissemination of scientific research documents, whether they are published or not. The documents may come from teaching and research institutions in France or abroad, or from public or private research centers.

L'archive ouverte pluridisciplinaire **HAL**, est destinée au dépôt et à la diffusion de documents scientifiques de niveau recherche, publiés ou non, émanant des établissements d'enseignement et de recherche français ou étrangers, des laboratoires publics ou privés.



Distributed under a Creative Commons CC BY 4.0 - Attribution - International License

1 Call for participation: Collaborative benchmarking of
2 functional-structural root architecture models.
3 The case of root water uptake.

4 Andrea Schnepf^{1,14,*}, Christopher K. Black², Valentin Couvreur³, Benjamin M.
5 Delory⁴, Claude Doussan⁵, Axelle Koch⁶, Timo Koch⁷, Mathieu Javaux^{1,3},
6 Magdalena Landl^{1,14}, Daniel Leitner⁸, Guillaume Lobet^{1,14}, Trung Hieu Mai¹,
7 Félicien Meunier^{9,10}, Lukas Petrich¹¹, Johannes A. Postma¹², Eckart Priesack¹³,
8 Volker Schmidt¹¹, Jan Vanderborght^{1,14}, Harry Vereecken^{1,14}, and Matthias
9 Weber¹¹

10 ¹ Institut für Bio- und Geowissenschaften: Agrosphäre (IBG-3),
11 Forschungszentrum Jülich GmbH, Wilhelm-Johnen-Str., D-52425 Jülich, Germany.

12 ²Department of Plant Science, The Pennsylvania State University, 102 Tyson
13 Building, University Park PA 16802, USA.

14 ³Earth and Life Institute, Agronomy, Université catholique de Louvain,
15 Louvain-la-Neuve, Belgium

16 ⁴Institute of Ecology, Leuphana University Lüneburg, Universitätsallee 1, 21335
17 Lüneburg, Germany.

18 ⁵UMR 1114 EMMAH, INRA/UAPV, 84914, Avignon cedex 9, France.

19 ⁶Earth and Life Institute, Environmental Sciences, Université catholique de
20 Louvain, Louvain-la-Neuve, Belgium

21 ⁷Department of Hydromechanics and Modelling of Hydrosystems, University of
22 Stuttgart, Pfaffenwaldring 61, 70569 Stuttgart, Germany.

23 ⁸Simulationswerkstatt, Ortmayrstrasse 20, A-4060 Leonding, Austria.

24 ⁹CAVELab - Computational and Applied Vegetation Ecology, Ghent University,
25 Ghent, Belgium.

26 ¹⁰Department of Earth and Environment, Boston University, Boston, USA.

27 ¹¹Institute of Stochastics, Ulm University, Helmholtzstr. 18, D-89069 Ulm,
28 Germany.

29 ¹²Institut für Bio- und Geowissenschaften: Plant Sciences (IBG-2),
30 Forschungszentrum Jülich GmbH, Wilhelm-Johnen-Str., D-52425 Jülich, Germany.

31 ¹³Institute of Soil Ecology, Helmholtz Zentrum München, Ingolstädter Landstr. 1,
32 85764 Neuherberg, Germany.

33 ¹⁴International Soil Modelling Consortium ISMC, Jülich, Germany

34 *Corresponding author, email: a.schnepf@fz-juelich.de

35 **Abstract**

36 Three-dimensional models of root growth, architecture and function are becoming im-
37 portant tools that aid the design of agricultural management schemes and the selection of
38 beneficial root traits. However, while benchmarking is common in many disciplines that use
39 numerical models such as natural and engineering sciences, functional-structural root archi-
40 tecture models have never been systematically compared. The following reasons might induce
41 disagreement between the simulation results of different models: different representation of
42 root growth, sink term of root water and solute uptake and representation of the rhizosphere.
43 Presently, the extent of discrepancies is unknown, and a framework for quantitatively compar-
44 ing functional-structural root architecture models is required. We propose, in a first step,

45 to define benchmarking scenarios that test individual components of complex models: root
46 architecture, water flow in soil and water flow in roots. While the latter two will focus mainly
47 on comparing numerical aspects, the root architectural models have to be compared at a conceptual
48 level as they generally differ in process representation. Therefore defining common
49 inputs that allow recreating reference root systems in all models will be a key challenge. In
50 a second step, benchmarking scenarios for the coupled problems are defined. We expect that
51 the results of step 1 will enable us to better interpret differences found in step 2. This benchmarking
52 will result in a better understanding of the different models and contribute towards
53 improving them. Improved models will allow us to simulate various scenarios with greater
54 confidence and avoid bugs, numerical errors or conceptual misunderstandings. This work will
55 set a standard for future model development.

56 1 Introduction

57 A growing number of different modelling techniques and software libraries are now available to
58 build functional-structural root architecture models. Different available models of root architecture
59 and functions have been discussed and qualitatively compared in Dunbabin et al. (2013).
60 The available models differ in the way they represent different processes such as root growth, water
61 flow, solute transport are captured and translated into mathematical equations (process-level
62 differences); in how they solve mathematical problems by their choice of analytical or numerical
63 approach, numerical scheme, programming technique (solution-level differences); and in how they
64 couple the different processes to the full model (coupling-level differences). However, the extent of
65 discrepancies is currently unknown. Thus, a framework for quantitatively comparing functional-
66 structural root architecture models is required. In addition to the explanatory or predictive power
67 of a model, it is also important to understand the performance of these models, e.g. in terms of
68 accuracy or computational cost. The most commonly used type of functional-structural root architecture
69 models represent the structure of the root system as a 1-dimensional branched network
70 of discrete segments which is geometrically embedded in a 3-dimensional soil domain (Koch et al.,
71 2018b). The root architecture may either be known from measurements, such as 2D or 3D images,
72 or from root architectural models. Suitable models are then used to simulate the "functions",
73 such as carbon flow and use in root systems (Bidel et al., 2000, e.g.), rhizodeposition (Nygren and
74 Perttunen, 2010), competition between species (Dun), plant anchorage (Dupuy et al., 2007), water
75 and nutrient uptake (Dunbabin et al., 2006; Javaux et al., 2008). Exchange between soil and root
76 is typically modelled via source/sink terms. From the point of view of the soil domain, roots are
77 often considered as line sources, i.e. it is assumed that their diameter is small compared to the
78 relevant spatial scale of the soil. The advantage of this approach is that it does allow to consider
79 root system architecture (position of each segment in time and 3D space) explicitly while being
80 computationally less expensive than an explicit representation of root volumes in the soil domain.
81 By direct comparison with explicit 3D simulations, Daly et al. (2017) showed that the error made
82 by neglecting root volumes physically present in the soil domain is negligibly small in case of root
83 water uptake. Thus, models of this type are sufficiently accurate and computationally cheaper than
84 explicit 3D. The challenge is now to develop a commonly accepted framework for benchmarking
85 functional-structural root architecture models. This includes defining a set of benchmark problems
86 to test model accuracy and performance. We propose that models should be evaluated against two
87 different kinds of references: First, we will develop simple benchmark scenarios, if possible with
88 analytical solutions, that serve as a reference for model verification. Secondly, we define data
89 sets that can be used as references for the evaluation of more complex models without analytical
90 solution. These data sets should as good as possible describe the system we want to model and
91 contain as little uncertainty as possible (Luo et al., 2012). This benchmark activity focuses on two
92 processes, root architecture development and root water uptake. We propose this benchmarking
93 framework to be used by the community of modellers and other participants to compare their
94 model outputs against those of the reference solutions of benchmarks defined in this paper. The
95 use of this framework thus aims to be a collaborative effort. We will refer to any numerical model
96 that implemented some or all of the benchmark problems as "participating model" or "simulator".

97 2 Benchmark problems for models of root architecture and 98 function

99 In order to benchmark models of root architecture and function, we propose a multi-step approach
100 with growing level of complexity. The individual benchmarks refer as much as possible to published
101 work, however, we streamlined the different problems and made the notation consistent throughout
102 this paper. A list of symbols is provided in Table 1. The intrinsic nature of functional-structural
103 root architecture models involves multiple coupled domains and processes. A single process in a
104 single domain (e.g. water flow in soil) is referred to as “module” here. The first set of benchmarks
105 (M1-M3) is about individual modules (M) only, i.e. they either deal with only root growth,
106 water flow in soil or water flow inside roots. The scenarios are simple, possibly have analytical
107 solutions, and the goal is to build trust in the accuracy of the individual participating models and
108 to help interpret potentially diverging results of the coupled benchmark problems. Benchmark
109 problems M1 are about root architecture development. It is known that the representation of
110 growth processes can be very different between different simulators. Thus, the goal is to calibrate
111 each simulator individually to given root image data (reference data). M2 is about modelling water
112 flow in soil. Here all participating models solve the same equation, namely the Richards equation,
113 and differences may occur due to differences in numerical implementation. M3 deals with water
114 flow inside the root system for static soil water conditions. As for M2, differences between models
115 are expected to be mainly due to the numerical implementation of this well defined process. The
116 second set of benchmarks (C1 and C2) is about coupled root-soil models. Benchmark problems C1
117 consider a static (non-growing) root system and focus on comparison of numerical representation of
118 agreed-upon equations and process representations as well as on the coupling approach to compute
119 the sink term for root water uptake. For this benchmark, we provide a reference solution that is
120 based on a computational mesh that was generated with consideration of the physical presence of
121 the roots in the soil domain. Thus, root water uptake was simulated not by a sink term but as a
122 boundary condition at the root surface in soil. Our approach is similar to Daly et al. (2017) but
123 in addition couples the soil domain to the root domain so that pressure gradients along the roots
124 are simulated. Benchmark problem C2 compares the water uptake of fully coupled models with
125 growing root systems.

126 Each benchmark problem is described in a Jupyter Notebook that is publicly available on a
127 github repository. We will provide codes for automatic analyses and comparison of different model
128 results with the reference solutions or reference data. This makes the analysis transparent and
129 easily modifiable and facilitates including even future participating models’ outputs at any later
130 time.

131
132 **Levels of contribution** Any group using or developing functional-structural root architecture
133 models is invited to participate in this collaborative model comparison. Not every model might be
134 suited for all of the provided benchmark problems. Thus, every participant may decide in which
135 individual benchmark problem they would like to participate. However, to reach a certain level of
136 complexity, the “module” benchmarks should be simulated first before the “coupled” benchmarks.
137 Table 2 gives an overview of the key features of these problems and their implementations. One
138 important aim of this activity is a joint publication that shows and discusses the results of the
139 different participating models in comparison to the reference solutions and reference data provided
140 as well as to gain an overview of the extent of deviations between the different simulators.

141 **How to participate** The participation includes three steps:

142
143 **(1) Registration** Any interested researcher is welcome to contact the corresponding author of
144 this paper, Andrea Schnepf, with the following information: Name, affiliation, name or reference
145 to the participating simulator. Upon signing a letter of agreement confirming that results of other
146 participants will not be published without consent, researchers will be accepted as participants and
147 enabled to include their individual simulation results to the github repository of this benchmark
148 initiative, <https://github.com/RSA-benchmarks/collaborative-comparison>.

149 **(2) Simulation** Each participant implements all or a selected number of benchmark problems in
150 their respective simulator and makes the results in the prescribed formats available to the github
151 repository through pull requests. Requested formats include RSML (Lobet et al., 2015) for root
152 architectures and VTK (Schroeder et al., 2006) for 3D and 1D simulation outputs. Python scripts

153 to read and write RSML files will be provided on the github repository. Packages to read and write
154 VTK files are for example available at <https://pypi.org/project/vtk/>.
155 **(3) Analysis and publication** The analysis of results and computation of relevant metrics, such
156 as root mean square error, coefficient of determination or Nash–Sutcliffe efficiency, will be done by
157 the code implemented in the Jupyter Notebooks for each benchmark problem. The final goal is to
158 jointly publish the results.

Table 1: List of notations

Symbol	Units	Description
d	cm	depth
D_w	cm^2d^{-1}	water diffusivity
\mathbf{e}_3	(0,0,1)	standard unit vector
J	$\text{cm}^3\text{cm}^{-2}\text{d}^{-1}$	water flux per unit soil surface area
k_r	$\text{cm}^3\text{cm}^{-2}\text{cm}^{-1}\text{d}^{-1}$	root radial conductivity (defined as volume of water per unit root surface area, pressure head gradient and time)
k_x	$\text{cm}^4\text{cm}^{-1}\text{d}^{-1}$	specific root axial conductance
$K(\theta)$	$\text{cm}^3\text{cm}^{-2}\text{d}^{-1}$	soil hydraulic conductivity
K_{sat}	$\text{cm}^3\text{cm}^{-2}\text{d}^{-1}$	saturated soil hydraulic conductivity
l	cm	length
n	-	van Genuchten shape parameter
q	$\text{cm}^3\text{cm}^{-2}\text{d}^{-1}$	water flux per unit root surface area
Q	cm^3d^{-1}	volumetric water flow rate
\bar{Q}	cm^3d^{-1}	daily average volumetric water flow rate
Q_r	cm^3d^{-1}	radial root water flow rate
Q_x	cm^3d^{-1}	axial root water flow rate
r_{root}	cm	root radius
S_w	$\text{cm d}^{-0.5}$	sorptivity (infiltration) or desorptivity (evaporation)
t	d	time
\mathbf{v}	(v_1, v_2, v_3)	normalised direction of the xylem, pointing towards the root tip
w	cm	width
x, y, z		spatial coordinates, z-axis pointing upward, soil surface is at $z=0$
Y	-	cumulative root fraction from surface to depth d
α	cm^{-1}	van Genuchten shape parameter
β	-	root distribution index
η	cm	position of the infiltration front (eqn. (4))
λ	-	van Genuchten-Mualem parameter
Λ	-	root domain (network of root center-lines)
Ω	-	soil domain
Φ	cm^2d^{-1}	matric flux potential
θ	$\text{cm}^3\text{cm}^{-3}$	volumetric water content
θ_a	$\text{cm}^3\text{cm}^{-3}$	reference water content
θ_{res}	$\text{cm}^3\text{cm}^{-3}$	residual water content
θ_{sat}	$\text{cm}^3\text{cm}^{-3}$	saturated water content
ψ	cm	water pressure head, described as potential energy per unit weight of water (i.e. units are cm of water column), given as relative to air pressure of 1020 cm and excluding the gravitational potential
ζ		local coordinate along root axis
sub indices		
collar	root collar (upper boundary of root system domain)	
i	initial	
pot	potential	
r	radial	
res	residual	
s	soil	
sat	saturation	
seg	root segment	
sim	simulation	
sur	soil surface	
tip(s)	root tip(s) (boundaries of root system domain)	
top	top, position of the soil surface	
out	outer radius of soil cylinder around a single root	
x	xylem	

Table 2: Description of benchmark scenarios to be implemented in 3D functional-structural root architecture models.¹

	Benchmark problem	Domain	Initial conditions	Boundary conditions	Evaluation	Remarks
RSA	M1.1: RSA calibration	$t_{sim}=11$ (8) for lupine (maize)	seed position (0,0,-3)	n.a.	Comparison against the measured root systems provided - traits and persistent homology (PH)	Model parameters are determined from calibration against traced images provided in the github repository in RSML format in the folder in M1.1 RSA calibration/M1.1 Reference data; 100 realisations for each model setup
	M1.2: RSA simulation	$t_{sim}=60$	seed position (0,0,-3)	n.a.	No reference solution, comparison amongst models - traits, PH, RLD	RSA model parameters from M1.1; 10 realisations for each model setup
Soil	M2.1: Infiltration	$1 \times w \times d = 10 \times 10 \times 200$, $t_{sim}=1$	$\psi_{s,i} = -400$	at $z = 0$ $\begin{cases} J_s = 100 \text{ if } \psi_s < 0 \\ \psi_s = 0 \text{ else} \end{cases}$, $\frac{\partial \psi_s}{\partial z} _{z=200} = 1$, no-flux at the sides	Analytical solution, eqn. (3)	sand, loam, clay (Table 3)
	M2.2: Evaporation	$1 \times w \times d = 10 \times 10 \times 100$, $t_{sim}=10$	$\psi_{s,i} = -40$ for sand and -200 for all other scenarios	at $z = 0$ $\begin{cases} J_s = J_{s,ref} \text{ if } \psi_s > -10,000 \\ \psi_s = -10,000 \text{ else} \end{cases}$, no-flux at all other boundaries	Analytical solution, eqn. (4)	scenario 1: sand, $J_{s,ref} = -0.1$, scenario 2: loam, $J_{s,ref} = -0.1$, scenario 3: loam, $J_{s,ref} = -0.3$, scenario 4: clay, $J_{s,ref} = -0.3$
Xylem	M3.1: Single root	1 vertical root, $L=50$	n.a.	$\psi_x _{collar} = -1000$, $Q_r _{tip} = 0$	Analytical solution, Eq. (11)	$k_x=0.0432$, $k_r=1.73 \times 10^{-4}$, $\psi_s = -200$
	M3.2: Root system	14-day old root system	n.a.	$\psi_x _{collar} = -500$, $Q_r _{tips} = 0$	Hybrid analytical solution (Meunier et al., 2017)	root hydraulic properties in scenario (a): Table 4, (b): Fig. 7, $\psi_s = -200$, static RSA given in the <code>root_grid</code> folder of this benchmark
Coupled 1	C1.1: Single RWU	1D radially symmetric, $r_{root} = 0.02$, $r_{out} = 0.6$, $t_{sim}=20$	$\psi_{s,i} = -100$	at $r = r_{root}$ $\begin{cases} q_r = q_{root}, \text{ if } \psi_s > -15,000 \\ \psi_s = -15,000 \text{ else} \end{cases}$, $q_r _{r=r_{out}} = 0$	Analytical solution, Eqs. (16) and (17)	sand, loam, clay (Table 3), scenarios 1-3: $q_{root}=0.1$, scenarios 4-6: $q_{root}=0.05$
	C1.2: RWU, static RSA	static 8-day old root system, soil: $1 \times w \times d = 8 \times 8 \times 15$, $t_{sim}=3$	$\psi_{s,i} = -659.8 - z$	$Q_r _{collar} = \begin{cases} Q_r = 6.4 \text{ if } \psi_s > -15,290 \\ \psi_s = -15,290 \text{ else} \end{cases}$, $Q_r _{tips} = 0$, no-flux at all soil faces	Reference solution: explicit 3D simulation	loam (Table 3), static RSA given in the <code>root_grid</code> folder of this benchmark, root hydraulic properties in scenario (a): Table 4, (b): Fig. 7
Coupled 2	C2.1: RWU, dynamic RSA	growing root system, soil: $1 \times w \times d = 25 \times 25 \times 100$, $t_{sim}=60$	$\psi_{s,i} = -200$	$Q_r _{collar} = \begin{cases} Q_r = 0.5 \cdot rel_{LAI} \text{ if } \psi_x > -15,000 \\ \psi_x = -15,000 \text{ else} \end{cases}$, $Q_r _{tips} = 0$, no-flux at all soil faces	No reference solution, comparison amongst models	loam (Table 3), $k_x=0.0432$, $k_r=1.73 \times 10^{-4}$, RSA parameters from M1.1, rel_{LAI} scales the potential transpiration

¹ All paths are relative to the github repository <https://github.com/RSA-benchmarks/collaborative-comparison.git>. For other abbreviations and units see Table 1.

160 2.1 Benchmarks for individual modules

161 2.1.1 Module M1: Root system architecture models

162 Root system architecture models (RSA models) are that module within a complex functional-
163 structural plant model that simulates the structure, topology, and 3D placement of the roots. They
164 simulate the growth of root systems as (upside down) tree-like structures based on rules regarding
165 elongation, branching and death. Mostly, they are discrete models and represent the root system
166 by a mathematical graph (i.e., nodes and edges/root segments). Each node or segment may be
167 additionally associated with attributes such as radius, age or hydraulic properties.

168 The aim of this first benchmarking exercise is to determine if root architecture models currently
169 available are able to reproduce realistic root architectures when being parameterised on the basis
170 of a common experimental data set (Fig. 2a). The particular challenge to benchmark RSA models
171 is to include the stochastic nature of these models. We propose to perform the benchmarking of
172 those models in four steps: (1) Parameterising the root architecture models based on the provided
173 experimental data, (2) Simulating a set of root systems for a dicotyledonous (*Lupinus albus*) and a
174 monocotyledonous (*Zea mays*) plant species following two benchmark scenarios (M1.1 and M1.2),
175 (3) Export and store the simulated root systems as Root System Markup Language (RSML) files
176 (Lobet et al., 2015), and (4) Compare the simulation results using the data analysis pipelines
177 available in the associated Jupyter Notebooks. The analysis pipelines are explained below and
178 illustrated in Fig. 1. In particular, we include persistent homology as an approach that augments
179 purely trait-based comparisons, i.e., two root systems with the same total root length could be
180 very different based on the persistent homology approach.

181 **M1.1 Root system architecture model calibration** The different available root architecture
182 models (see e.g. Dunbabin et al., 2013) are partly different in the way they represent the growth
183 processes, i.e. we are looking at process-level differences between the different models. Thus, each
184 participating RSA model will have a different set of parameters that drive root growth. This is the
185 reason why, in this benchmark, we do not prescribe a parameter set as in e.g. M2 or M3, but we
186 let each participating model derive its respective model parameters based on a reference dataset.
187 In this first benchmark (M1.1), modellers simulate root systems for the same duration as the age
188 of the root systems in the reference dataset.

189 **Reference data set** Although the parameterisation of 3D models using a set of parameters
190 derived from 2D images has some limitations, it has been shown to be a simple and efficient strategy
191 allowing the simulation of realistic 3D root systems (Landl et al., 2018). Our reference dataset
192 contains two distinct sets of images: (1) images of lupin roots grown for 11 days in an aeroponic
193 setup (Lobet et al., 2011), and (2) images of maize roots grown for 8 days on filter papers (Hund
194 et al., 2009). All images were analysed using the semi-automated root image analysis software
195 SmartRoot (Lobet et al., 2011) and root tracings were saved as RSML files for further analysis
196 (Fig. 1). These RSML files were then processed using functions of the R package archiDART
197 developed to compute root system- and single root-level metrics (Delory et al., 2016, 2018). These
198 metrics have been made open-access (https://github.com/RSA-benchmarks/collaborative-comparison/tree/master/root_architecture/data) and should help modellers to parameterise
199 their respective RSA model.
200

201 **Required output** The following results are to be uploaded via pull requests to this path
202 on the github repository: M1 Root architecture development/M1.1 RSA calibration/M1.1
203 Numerical results.

- 204 1. A text file including the outcome of the calibration step, i.e., the set of model input parameters
205 required for the specific simulator.
- 206 2. Simulation output from running the root architecture model using this parameter set in
207 RSML format. Due to the stochastic nature of root architecture models, 100 realisations of
208 each model setup are requested. The file format should be RSML and the file name should
209 be of the form "modelname_replicate", e.g. "CRootBox_1.rsm1".

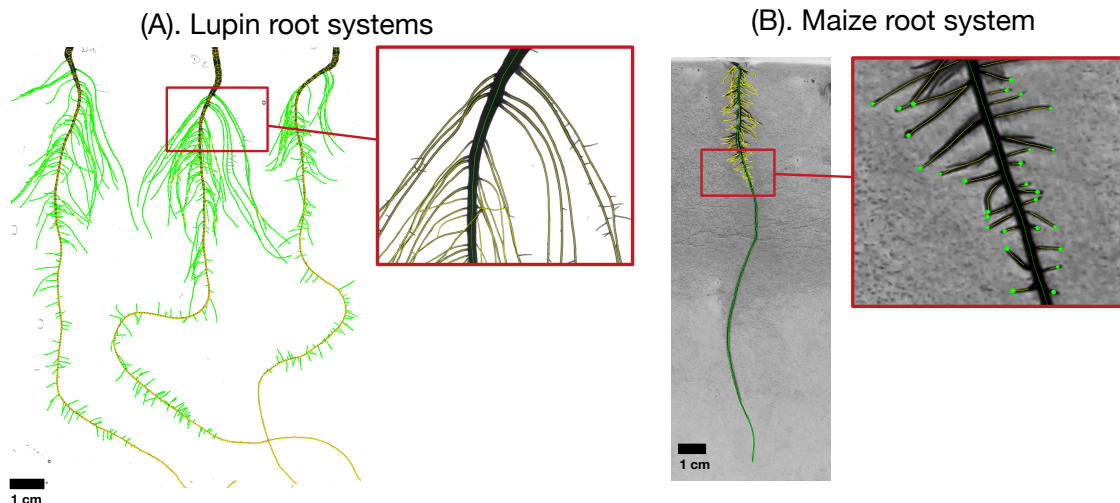


Figure 1: Example of root images used for the benchmarking dataset. Panel (A) shows an image of lupin root systems, 11 days old, growing in an aeroponic setup. Panel (B) shows an image of a maize root system growing on filter paper (5 days old). All images were analysed using the semi-automated root image analysis software SmartRoot (Lobet et al., 2011), colours distinguish different root orders. The RSML files containing the full information about the root systems are provided on the github repository in the folder "M1.1 RSA calibration\M1.1 Reference data".

210 **Reference data analysis and automated model comparison** Statistical evaluation of a
211 root architecture model has for example been done by Schnepf et al. (2018); Delory et al. (2018).
212 This motivated the creation of two data analysis pipelines for the first benchmark (M1.1) that
213 will be used to compare simulation outputs with reference experimental data (reference root sys-
214 tems) (Fig. 2a). These two data analysis pipelines are implemented in the Jupyter Notebook
215 `RSA calibration.ipynb` that can be found on the github repository that contains code that will
216 automatically include every model output in the analysis that is available in the prescribed folder.
217 The analysis relies on the functions available in the **R** package `archiDART` (Delory et al., 2016,
218 2018). In the first pipeline, traits computed at the root system level (e.g., total root system
219 length, number of roots per branching order) are compared between all simulated and reference
220 root systems. This comparison takes place in three steps: (1) identifying the key morphological,
221 architectural, and topological (Fitter indices, Fitter 1987; Fitter and Stickland 1991) traits ex-
222 plaining differences between simulated and reference root systems using multivariate data analysis
223 techniques (e.g., discriminant analysis and principal component analysis), (2) looking at the point
224 in time, beyond the time period for which there are measurements, when simulated and reference
225 root systems start to diverge/converge with regard to the key root system traits identified in the
226 previous step and how large these differences are, and (3) assess the degree of dissimilarity between
227 simulated and reference root systems using dissimilarity metrics based on the raw data (Janssen
228 and Heuberger, 1995).

229 In the second pipeline, dissimilarities in architecture between reference and simulated root sys-
230 tems are compared using persistent homology. Persistent homology is a topological framework
231 that has proven to be a very powerful tool for capturing variations in plant morphology at dif-
232 ferent spatial scales (Li et al., 2017, 2018). The main output of a persistent homology analysis
233 is a persistence barcode recording the appearance and disappearance of each root branch when
234 a distance function traverses the branching structure (see Fig. 1 in Delory et al., 2018). The
235 degree of similarity between different root system topologies can be assessed by computing a pair-
236 wise distance matrix to compare persistence barcodes. In addition, Delory et al. (2018) showed
237 that both trait-based and persistent homology approaches nicely complement each other and allow
238 root researchers to more accurately describe differences in root system architecture (Delory et al.,
239 2018). In our data analysis pipeline, a persistent homology analysis comprises the following steps:
240 (1) computing a persistence barcode for each simulated and reference root system using a geodesic
241 distance function, (2) computing dissimilarities between persistence barcodes using a bottleneck
242 distance, (3) visualize dissimilarities between root systems using multidimensional scaling, and

243 (4) test specific hypotheses using permutational multivariate analysis of variance (PERMANOVA)
244 (Anderson, 2001).

245 **M1.2 Long model simulations** In this benchmark, modellers use the same input parameter
246 set as in M1.1, but simulate root system growth and development for a longer time period (60
247 days). The aim of this second benchmarking exercise is to assess if the different models diverge (or
248 converge) if simulations are run for a longer time period and extrapolate beyond the provided data
249 set (Fig. 2b). This is of great importance, as parameterisation of RSA models is often based on
250 relatively young plants, whereas knowledge of RSA of older root systems is scarce. Therefore, for
251 this M1.2 scenario, experimental data are not used as the basis of comparison anymore. It has to
252 be noted that these two benchmark problems focus on root architecture dynamics modelling only,
253 thus effect of soil properties on root growth is not explicitly modelled.

254 **Required output** The following results are to be uploaded via pull requests to this path on
255 the github repository: M1 Root architecture development/M1.2 RSA simulation/M1.2 Numerical
256 results.

- 257 1. A text file including the model input parameters used for the specific simulator.
- 258 2. Simulation output from running the root architecture model using this paramter set in RSML
259 format. Due to the stochastic nature of root architecture models, 100 realisations of each
260 model setup are requested. The file file format should be RSML and the file name should be
261 of the form "modelname_replicate", e.g. "CRootBox_1.rsml".

262 **Analysis pipeline for M1.2** For the second benchmark (M1.2), three data analysis pipelines
263 are used to compare simulation outputs given by different root architecture models. For this
264 benchmark, the reference experimental data cannot be used as a reference as data of 60 day old
265 plants is not available. The first two data analysis pipelines for M1.2 are very similar to the ones
266 described earlier for the M1.1 benchmark. First, model outputs are compared using morphological,
267 architectural, and topological traits computed at the root system level. Second, differences in root
268 system morphology are analysed using persistent homology. In addition to these two analysis
269 pipelines, we included a third one to analyse differences in vertical root distribution between root
270 systems simulated with different root architecture models. To do so, we use the modelling approach
271 described in Oram et al. (2018). Briefly, relative cumulative root length density ($Y(d)$) is computed
272 using Eq. (1)

$$Y(d) = \sum_{i=0}^{i=d} RLD(i) / \sum_{i=0}^{\infty} RLD(i) \quad (1)$$

273 Eq. (2) is fitted to the computed $Y(d)$ using a non-linear least square means fitting procedure.
274 The fitting constant β is used to compare modeled rooting depth, with high β corresponding to
275 deep rooting.

$$Y(d) = 1 - \beta^d, \quad (2)$$

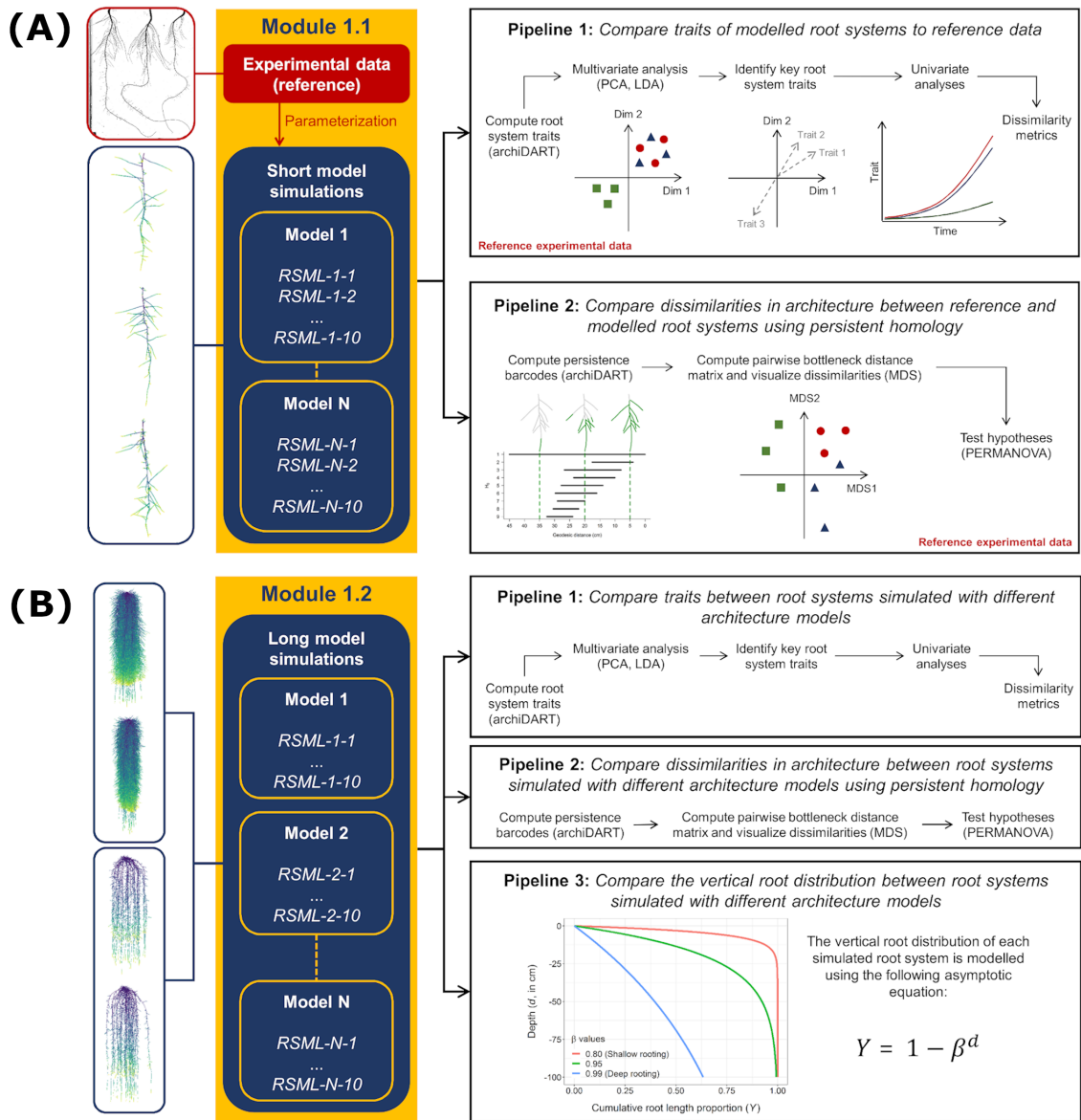


Figure 2: Presentation of the data analysis pipelines used for the benchmarking of root architecture models. Panels a and b show the first (M1.1) and second (M1.2) benchmark scenarios, respectively.

276 2.1.2 Module 2: Water flow in soil only

277 In this module, we describe benchmark problems that only relate to water flow in soil. Water flow
 278 in soil is most commonly described by the Richards equation in three dimensions:

$$\frac{\partial \theta}{\partial t} = \nabla \cdot (K(\theta) (\nabla \psi_s + \mathbf{e}_3)), \quad (3)$$

279 where θ is the volumetric soil water content ($\text{cm}^3 \text{cm}^{-3}$), K is the hydraulic conductivity (cm
 280 day^{-1}), ψ_s is the soil water pressure head (cm), and $\mathbf{e}_3 = (0, 0, 1)$ is the downward unit vector.

281 The relationship between soil water pressure head and water content is generally described by
 282 the water retention curve. In the following we will use the van Genuchten equation (Van Genuchten,
 283 1980) to describe this curve specifying the soil moisture characteristic of specific soils.

284 We expect differences between the outputs of different simulators to be mainly numerical
 285 solution-level differences, i.e., due to numerical scheme and implementation. Different numer-
 286 ical solutions of the Richards equation have been analysed before, and for some settings analytic
 287 solutions exist. We will use the benchmarks presented by Vanderborcht et al. (2005) to benchmark
 288 the part of the participating functional structural root architecture models where water movement

289 in soil is described. The analytical solutions provided in that paper are related to vertical changes
 290 in the soil profile only. As most functional-structural root architecture models have a 3D soil mod-
 291 292 and width for the numerical implementation of those problems.

293 In the following we will describe the benchmarks for water movement in soil. Table 3 gives an
 294 overview of the soil hydraulic properties that will be used throughout all the benchmarks involving
 water flow in soil.

Table 3: Soil hydraulic taken from Vanderborght et al. (2005). θ_{res} is the residual water content, θ_{sat} is the saturated water content, α and n are the van Genuchten parameters, K_{sat} is the saturated soil hydraulic conductivity and λ is the van Genuchten-Mualem parameter

Soil type	θ_{res} (-)	θ_{sat} (-)	α (cm^{-1})	n (-)	K_s (cm d^{-1})	λ (-)
sand	0.045	0.43	0.15	3.0	1000	0.5
loam	0.08	0.43	0.04	1.6	50	0.5
clay	0.1	0.40	0.01	1.1	10	0.5

295

296 **M2.1: Infiltration** This benchmark scenario is taken from Vanderborght et al. (2005). All
 297 parameters, initial and boundary conditions are given in Table 2 and are described below. For
 298 each of the soil types, sand, loam and clay, we consider the rate of infiltration into a soil with an
 299 initial homogeneous soil water pressure head of $\psi_s = -400$ cm. All profiles are 200 cm deep, at the
 300 top boundary we prescribe a constant influx of 100 cm d^{-1} as long as the soil is still unsaturated,
 301 and a Dirichlet boundary condition of $\psi_s = 0$ cm as soon as the soil is fully saturated. At the
 302 bottom boundary, we prescribe free drainage. Since this problem only produces gradients in the
 303 vertical direction, we compare numerical model results with the 1D analytical solution described
 304 in Vanderborght et al. (2005).

305 **Reference solution** The analytical solution is given by the travelling wave equation

$$\Delta\eta(\theta) = \eta(\theta) - \eta(\theta_a) = (\theta_{sur} - \theta_i) \int_{\theta}^{\theta_a} \frac{D_w(\theta)d\theta}{[K(\theta_{sur}) - K(\theta_i)](\theta - \theta_i) - [K(\theta) - K(\theta_i)](\theta_{sur} - \theta_i)}, \quad (4)$$

306 where D_w is the water diffusivity (defined as $D_w = K(\theta)\frac{\partial\psi_s}{\partial\theta}$), θ_{sur} is the water content at the
 307 soil surface, θ_i is the initial water content, θ_a is a reference water content (taken to be $\theta_a =$
 308 $(\theta_{sur} + \theta_i)/2$), $\eta = |z| - \frac{[K(\theta_{sur}) - K(\theta_i)]t}{\theta_{sur} - \theta_i}$ and $\Delta\eta(\theta)$ is the distance of the front to the the position
 309 of the reference water content. The implementation of this analytical solution, implemented in the
 310 Jupyter Notebook **M2.1 Benchmark problem.ipynb**, reproduces Figure 4abc from Vanderborght
 311 et al. (2005), where the water content is plotted after 0.1, 0.2, and 0.3 days for the sand scenario;
 312 0.2, 0.5, and 1 days for the loam scenario; and 0.1, 0.2, and 0.5 days for the clay scenario (see Fig.
 313 (3)).

314 **Required output** The following simulation results of participating models are to be up-
 315 loaded via pull requests to this path on the github repository: **M2 Water flow in soil/M2.1**
 316 **Infiltration/M2.1 Numerical results**.

- 317 1. A text file consisting of two rows containing comma separated depth values (cm) in the first,
 318 and water content ($\text{cm}^3\text{cm}^{-3}$) in the second for each time point and infiltration scenario (i.e.
 319 3 (time points) \times 3 (scenarios) results = 18 rows). The file name should be of the form
 320 "simulatorname.txt", e.g. "DuMux.txt".

321 Note that we do not prescribe spatial or temporal resolution of the outputs, as that may depend
 322 on the individual numerical schemes.

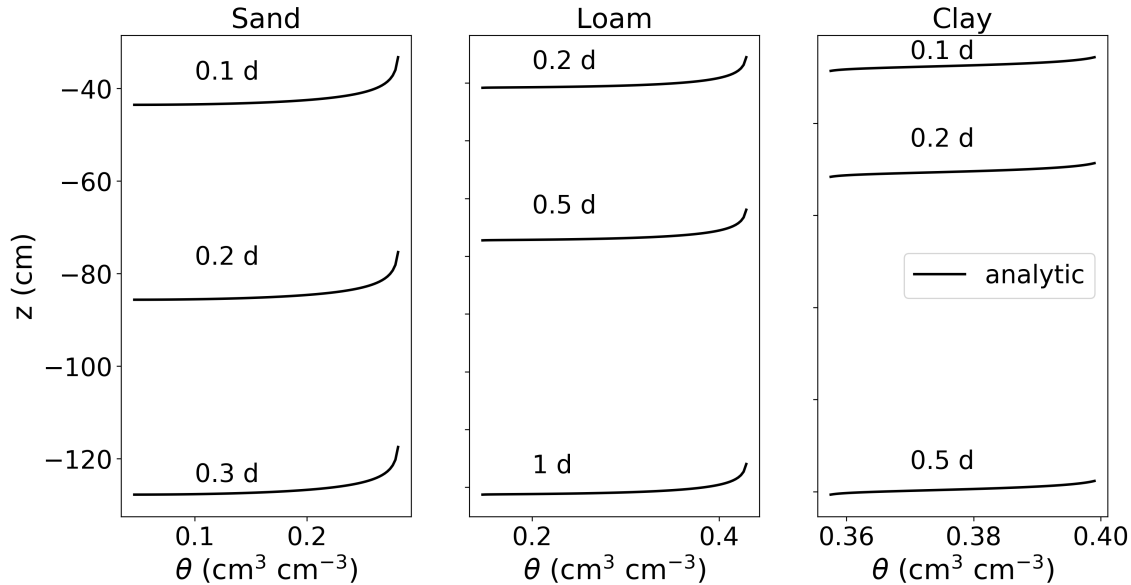


Figure 3: Results of M2.1: Infiltration into three initially dry soils: sand, loam and clay.

323 **M2.2: Evaporation** This benchmark reproduces Fig. (5) of Vanderborght et al. (2005). We
 324 consider four scenarios (sand, loam 1, loam 2, clay) in which we are interested in the actual
 325 evaporation over time from an initially moist soil ($\psi_i = -40\text{cm}$ for the sand scenario and ψ_i
 326 $= -200\text{cm}$ for all other scenarios). The domain is 100 cm deep with a width and length of 10 cm.
 327 At the top boundary, we prescribe a constant efflux of $J_{s,pot}=0.1 \text{ cm d}^{-1}$ for the sand and loam 1
 328 scenario, and 0.3 cm/day for the loam 2 and clay scenarios, at the bottom we prescribe zero-flux.
 329 When the soil reaches a critical soil water pressure head of -10.000 cm at the surface, we switch to
 330 a Dirichlet boundary condition with $\psi_s = -10.000 \text{ cm}$.

331 **Reference solution** The analytical solution to this problem is given by

$$J_s(z=0, t) = \begin{cases} J_{s,pot} & \text{for } t < t_{pot} \\ \frac{S_w(\theta_{sur}, \theta_i)}{2\sqrt{t' + t - t_{pot}}} & \text{for } t \geq t_{pot} \end{cases} \quad (5)$$

332 where $t' = \frac{S_w^2(\theta_{sur}, \theta_i)}{4J_{s,pot}^2}$, $t_{pot} = \frac{S_w^2(\theta_{sur}, \theta_i)}{2J_{s,pot}^2}$, $S_w(\theta_i, \theta_{sur}) = (\theta_i - \theta_{sur}) \sqrt{\frac{4}{\mu} \int_0^1 D_w(\Theta) d\Theta}$, $\Theta = \left| \frac{\theta - \theta_{sur}}{\theta_i - \theta_{sur}} \right|$,
 333 $\mu = \frac{3\beta \left(1 + \left\{ 1 - \frac{14}{9} \left[1 - \frac{\alpha}{(1-\beta)^2} \right] \right\}^{0.5} \right)}{2(1-\beta) \left[\frac{\alpha}{(1-\beta)^2} - 1 \right]}$, $\alpha = \frac{\int_0^1 (1-\beta\Theta)^2 D_w(\Theta) d\Theta}{\int_0^1 D_w(\Theta) d\Theta}$, and $\beta = \left[\frac{\int_0^1 \Theta D_w(\Theta) d\Theta}{\int_0^1 D_w(\Theta) d\Theta} \right]^2$. Fig. (4) shows
 334 the rate of evaporation over time for the four scenarios soil, loam 1, loam 2, clay.

335 **Required output** The following simulation results of participating models are to be up-
 336 loaded via pull requests to this path on the github repository: M2 Water flow in soil/M2.2
 337 Evaporation/M2.2 Numerical results.

338 1. A text file consisting of two rows containing comma separated depth values (cm) in the first,
 339 and root pressure head (cm) in the second for each scenario (i.e. 4 (scenarios) \times 2 (rows) =
 340 8 rows). The file name should be of the form "simulatorname.txt", e.g. "DuMux.txt".

341 Note that we do not prescribe spatial or temporal resolution of the outputs, as that may depend
 342 on the individual numerical schemes. It is the responsibility of each participant, to upload the best
 343 possible solution.

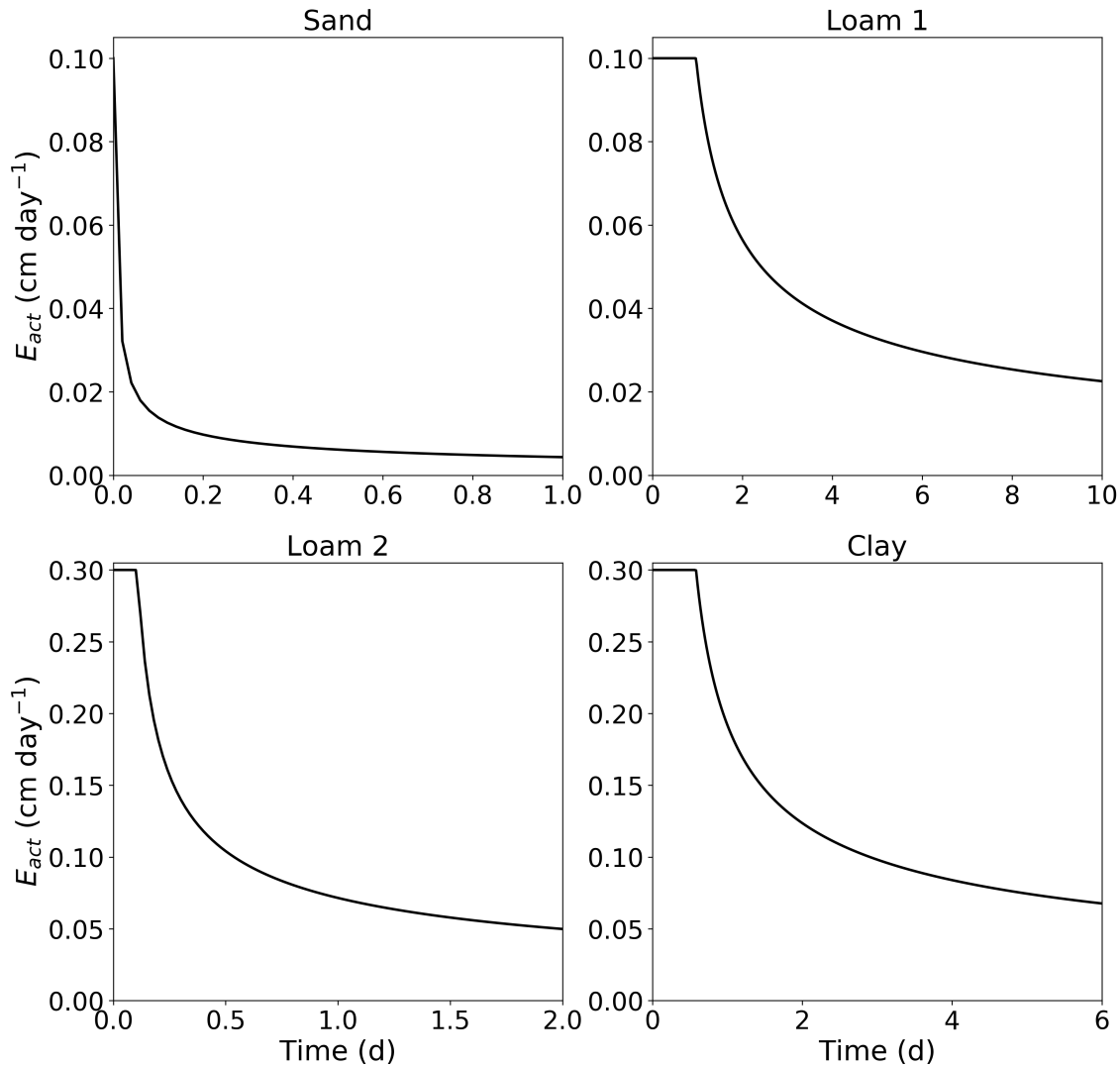


Figure 4: Results of M2.2: Rate of evaporation with respect to time from sand with $J_{s,pot}=0$ 1cm/d, loam with $J_{s,pot}=0$ 1cm/d, loam with $J_{s,pot}=0$ 3cm/d and clay with $J_{s,pot}=0$ 3cm/d

344 2.1.3 Module 3: Water flow in roots

345 In this benchmark, we consider water flow in xylem with constant and homogeneous soil water
 346 pressure head. This problem is well described, e.g., in Roose and Fowler (2004) and Doussan et al.
 347 (1998). Its analytical solution for a single root was already derived by Landsberg and Fowkes
 348 (1978). In Appendix A, we present a derivation that is equivalent to the solution of Landsberg and
 349 Fowkes (1978) but uses exponential instead of hyperbolic functions. Briefly, conservation of mass
 350 in a branched root network with both axial and radial water flow, neglecting plant water storage
 351 and osmotic potential, yields Eq. (6),

$$2r_{root}\pi k_r(\psi_s - \psi_x) = -k_x \frac{\partial^2 \psi_x}{\partial \zeta^2}, \quad (6)$$

352 where r_{root} is the root radius (cm), k_r is the radial conductivity (d^{-1}), ψ_s is the soil water pressure
 353 head of the surrounding soil (cm), ψ_x is the root water pressure head inside the xylem (cm), k_x is
 354 the axial conductance ($cm^3 d^{-1}$), and ζ is the axial coordinate (cm).

355 **M3.1: A single root in static soil with constant root hydraulic properties** In this
 356 benchmark problem, we assume a vertical single straight root segment surrounded by a soil with a
 357 constant and uniform soil water pressure head (i.e. the soil is not in hydrostatic equilibrium). We

358 prescribe the root water pressure head at the root collar as $\psi_x|_{\text{collar}} = \psi_0$, and no axial flow at the
 359 root tips.

360 **Reference solution** For constant k_r and k_x we can solve Eq. (6) yielding

$$\psi_x(\zeta) = \psi_s + d_1 e^{\sqrt{c}\zeta} + d_2 e^{-\sqrt{c}\zeta}, \quad (7)$$

with $c = 2r_{\text{root}}\pi k_r/k_x$. The integration constants d_1 and d_2 for above boundary conditions are given by

$$d_1 = d^{-1} \left(e^{-\sqrt{c}l_{\text{seg}}} (\psi_0 - \psi_s) + 1 \right) \quad (8)$$

$$d_2 = -d^{-1} \left(e^{\sqrt{c}l_{\text{seg}}} (\psi_0 - \psi_s) + 1 \right), \quad (9)$$

$$(10)$$

where l_{seg} is the segment length, and d is the determinant of above matrix

$$d = e^{-\sqrt{c}l_{\text{seg}}} - e^{\sqrt{c}l_{\text{seg}}}, \quad (11)$$

361 see Appendix A. Fig. 5 shows the analytical solution to this benchmark using the parameters given
 362 in Table 4.

Table 4: Parameters of scenario M3.1.

l	50	length of a single straight root (cm)
r_{root}	0.02	radius (cm)
k_z	4.32×10^{-2}	axial conductivity ($\text{cm}^3 \text{d}^{-1}$)
k_r	1.73×10^{-4}	radial conductivity (d^{-1})
ψ_s	-200	static soil water pressure head (cm)
ψ_0	-1,000	Dirichlet boundary conditions at the root collar (cm)

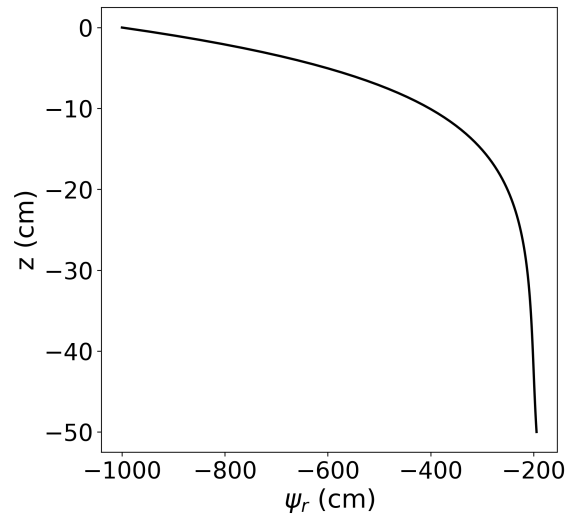


Figure 5: Results of M3.1: Root water pressure head distribution within a single vertical root

363 **Required output** The following simulation results of participating models are to be uploaded
 364 via pull requests to this path on the github repository: M3 Water flow in roots/M3.1 Single
 365 root/M31 Numerical results/.

366 1. A text file consisting of two rows containing comma separated depth values (cm) in the
 367 first, and root pressure head (cm) in the second. The file name should be of the form
 368 "simulatorname.txt", e.g. "DuMux.txt".

369 Note that we do not prescribe spatial resolution of the outputs, as that may depend on the indi-
 370 vidual numerical schemes.

371 **Benchmark M3.2: A small root system in a static soil** In the following benchmark, we
372 extend benchmark M3.1 from a single root to a root system. We consider water flow inside a small
373 static root system of a lupine plant which was grown for 14 days in a soil-filled column of 20 cm
374 depth and 7 cm diameter. The root system was imaged by MRI at Forschungszentrum Jülich; the
375 segmented root structure is provided in RSML, DGF (Dune grid format) (Bastian et al., 2008)
376 and RSWMS (Javaux et al., 2008) formats in the folder M3 Water flow in roots/M3.2 Root
377 system/root_grid on the github repository. It is visualised in Fig. 6(a,b) with colours denoting
378 root order and root segment age.

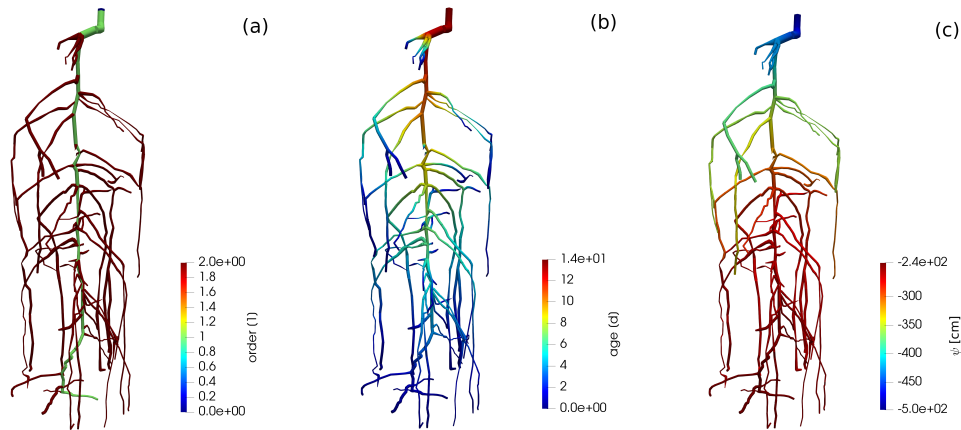


Figure 6: Visualisation of the root system of M3.2 with colours denoting (a) root order, (b) root segment age, (c) root water pressure head.

379 **Reference solution** The reference solution for this problem is given by the hybrid analytical-
380 numerical solution of water flow in the root hydraulic architecture proposed by Meunier et al.
381 (2017). The advantage of this solution is that it is independent of the spatial resolution of the root
382 system (i.e. root segment length).

383 We consider two scenarios. The first one uses the same constant root hydraulic properties
384 as given in Table 4, i.e. considering the same root hydraulic properties for each root segment.
385 In the second scenario, we consider age-dependent root hydraulic properties for tap root and
386 laterals of lupine as obtained by Zarebanadkouki et al. (2016, exponential function scenario) and
387 converting distance from root tip to root age by assuming a root growth rate of 1 cm d^{-1} . This
388 parameterisation takes into account that roots get a higher axial conductivity and lower radial
389 conductivity as they are becoming older (see Fig. 7, a table with the actual values is provided on the
390 github repository, in: M3 Water flow in roots/M3.2 Root system/M3.2 Benchmark problem.
391 ipynb).

392 A sample 3-D visualisation of the model output is shown in Fig. 6(c) for the constant root
393 hydraulic properties scenario. Fig. 8 shows the effect of constant and age-dependent root hydraulic
394 properties under otherwise same (soil and boundary) conditions.

395 **Required output** The following simulation results of participating models are to be uploaded
396 via pull requests to this path on the github repository: M3 Water flow in roots/M3.2 Root
397 system/M32a Numerical results and M3 Water flow in roots/M3.2 Root system/M32b Numerical
398 results for the constant and age-dependent root hydraulic properties cases.

- 399 1. A text file consisting of two rows containing comma separated depth values (cm) in the
400 first, and root pressure head (cm) in the second. The file name should be of the form
401 "simulatorname.txt", e.g. "DuMux.txt".

402 Note that we do not prescribe spatial resolution of the outputs, as that may depend on the indi-
403 vidual numerical schemes.

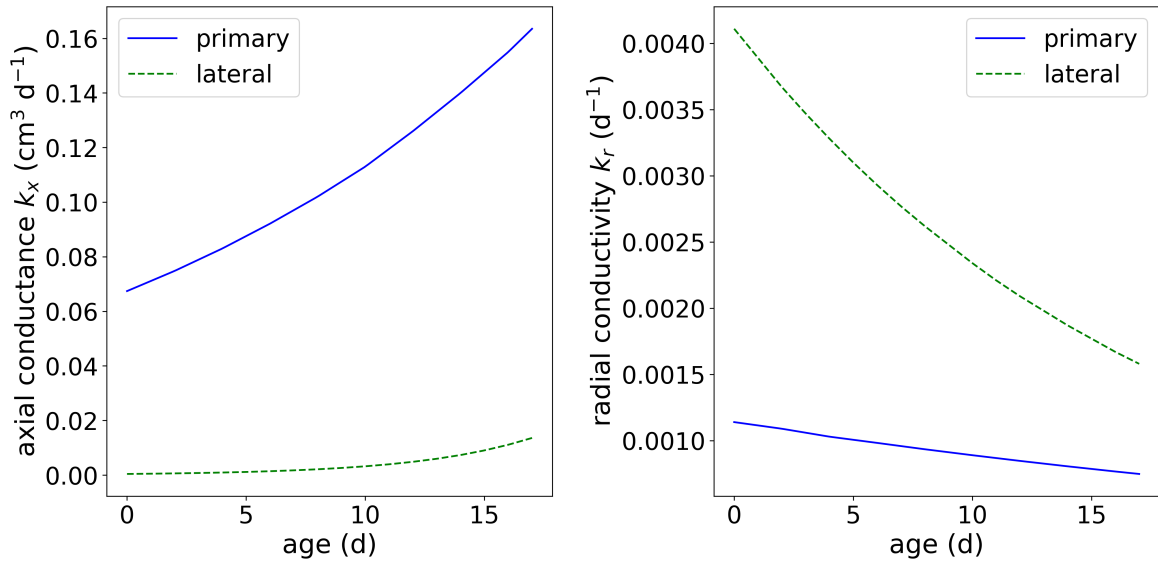


Figure 7: Root hydraulic properties dependency on root type and root segment age.

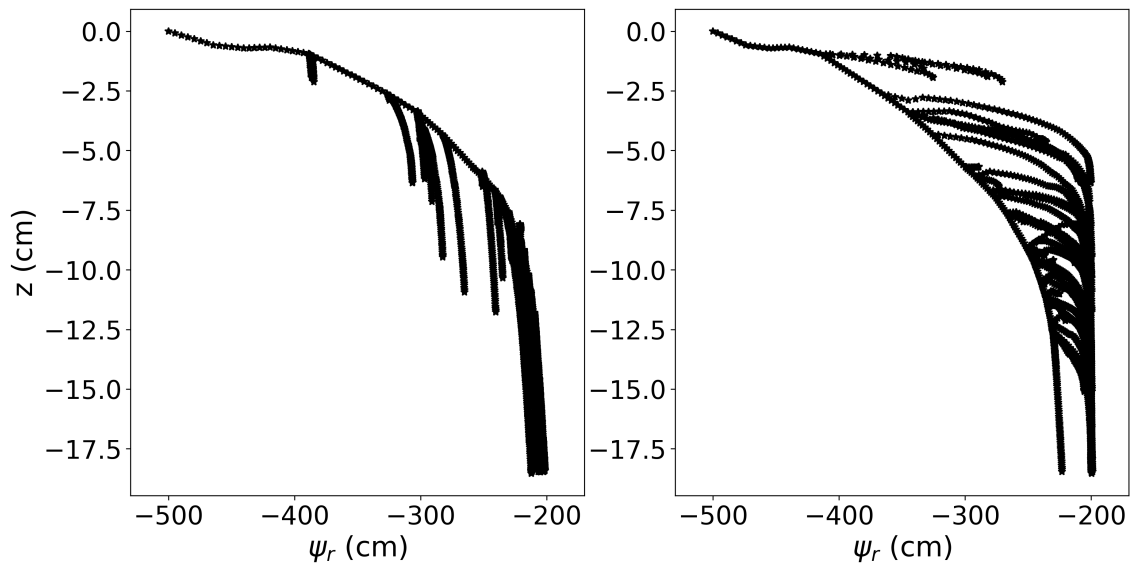


Figure 8: Results of M3.2. Left panel: Xylem pressure in each root segment of a root system with constant hydraulic properties. Right panel: Xylem pressure in each root segment of a root system with age-dependent hydraulic properties.

404 2.1.4 Coupled benchmark scenarios C1: Root water uptake by a static root system

405 The way of coupling can easily introduce differences in simulated results because of numerical
 406 errors (especially when there is two way coupling) or because different assumption are made when
 407 implementing the coupling. No analytical solutions exists for the coupled problems presented here,
 408 but the coupling (C) benchmarks are intended to quantify differences between model outputs of
 409 coupled models. We may see differences observed in the non-coupled benchmarks to be amplified,
 410 or to be irrelevant for the coupled problem.

411 **C1.1: Water uptake by a single root** This benchmark follows the paper of Schröder et al.
 412 (2008). Here we aim to see to what extent the different participating models can reproduce the
 413 hydraulic conductivity drop near the root surface under different soil conditions and transpiration
 414 demands. Thus, it requires the participating line-source based models to strongly increase the
 415 spatial resolution of the 3D soil domain. From this benchmark, we will learn, whether the spatial

416 resolution required to reproduce radial soil water pressure head gradients would be in a feasible
 417 order of magnitude for larger soil-root systems or not. If not, there are approaches to estimate
 418 soil water pressure head drop at the root-soil interface from bulk soil values as e.g. in Mai et al.
 419 (2019); Beudez et al. (2013), see also benchmark C1.2.

420 **Reference solution** The analytical solution is based on the analytical solutions of the 1D radially
 421 symmetric problem of water uptake by a single root, in which root water uptake is described as
 422 a boundary condition at the root-soil interface. We consider here two water uptake regimes, a
 423 non-stressed condition with maximum root uptake (q_{root}), and a stressed condition with a limiting
 424 plant root water potential constraining uptake. Based on the steady-rate assumption and using
 425 the matric flux potential $\Phi(h_c) = \int_{-\infty}^{h_c} K(h)dh$ that linearises the Richards equation, the radial soil
 426 water pressure head profiles for non-stressed and stressed conditions (stress conditions are given
 427 when the soil water pressure head at the root surface reaches $-15\,000\text{cm}$) are given by

$$\Phi_{nostress}(r) = \Phi_{r_{out}} + (q_{root}r_{root} - q_{out}r_{out}) \left[\frac{r^2/r_{root}^2}{2(1-\rho^2)} + \frac{\rho^2}{1-\rho^2} \left(\ln \frac{r_{out}}{r} - \frac{1}{2} \right) \right] + q_{out}r_{out} \ln \frac{r}{r_{out}} \quad (12)$$

428 and

$$\Phi_{stress}(r) = \left(\Phi_{r_{out}} - \Phi_{r_{root}} + q_{out}r_{out} \ln \frac{1}{\rho} \right) \frac{r^2/r_{root}^2 - 1 + 2\rho^2 \ln r_{root}/r}{\rho^2 - 1 + 2\rho^2 \ln 1/\rho} + q_{out}r_{out} \ln \frac{r}{r_{root}} + \Phi_{r_{root}}, \quad (13)$$

429 where $\rho = \frac{r_{out}}{r_{root}}$.

Given the soil water pressure head at the outer boundary, the solution computes the soil water pressure head profile towards the root. Due to the steady-rate assumption, the problem has become a stationary boundary value problem. However, under non-stressed conditions, we can calculate the time that corresponds to a given radial soil water pressure head profile by dividing the volume of water removed from the soil domain by the known water flow rate. The water remaining in a 1 cm long hollow cylinder around the root is given by

$$V = \int_0^{2\pi} \int_{r_{root}}^{r_{out}} r \theta dr d\phi = 2\pi \int_{r_{root}}^{r_{out}} r \theta dr$$

, θ being the water content. The initially available water volume in the soil domain is given by

$$V_i = (r_{out}^2 - r_{root}^2) \pi \theta_i.$$

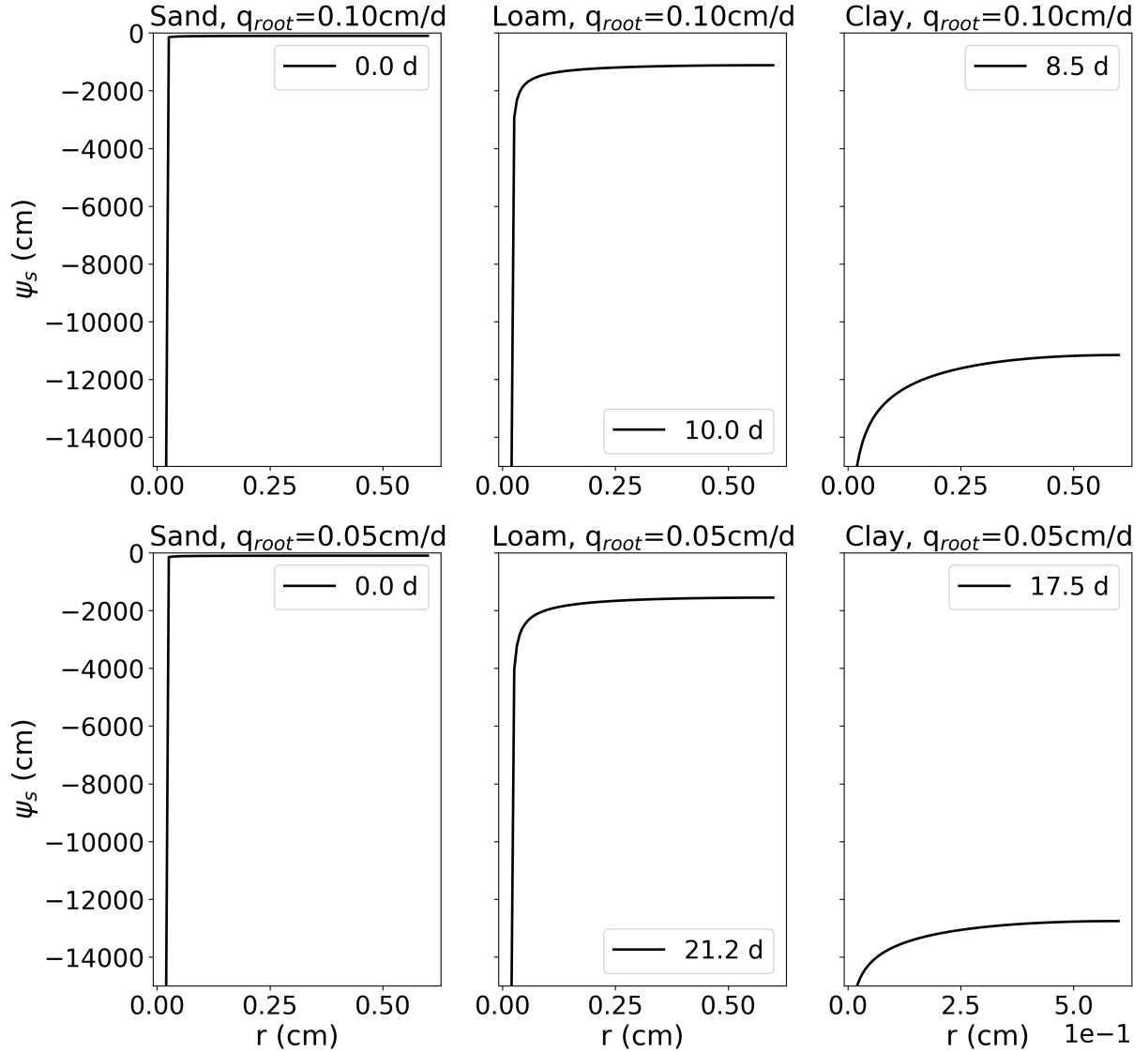
Thus, until the onset of stress, the corresponding time at which a given radial profile is reached is given by

$$t = \frac{(V_i - V)}{2r_{root}\pi q_{root}}.$$

430 For the three soils sand, loam, and clay (Table 3), we compute the analytical solution with the
 431 following parameters: $r_{root} = 0.02\text{cm}$, $r_{out} = 1\text{cm}$, $q_{root} = 0.5\text{cm/d}$, $\psi_{s,lim} = -15000\text{cm}$, $q_{out} =$
 432 0cm/d and for different soil water pressure heads at the outer end of the cylinder. Fig. 9 shows the
 433 soil water pressure head gradients at the onset of stress (i.e., when the soil water pressure head at
 434 the root surface reached $-15\,000\text{cm}$) and the time of its occurrence. The value of the initial water
 435 content is taken to be $\theta_i = -100\text{cm}$. This analytical solution is for radial water flow in soil towards
 436 the root only, i.e., not considering gravity or water flow inside the roots. Ideally, in their numerical
 437 implementation of this benchmark, the different participating models will turn off gravity effects.
 438 The soil domain for this numerical implementation has a size of $l \times w \times d = 1 \times 1 \times 1\text{ cm}$. The
 439 horizontal spatial resolution is high enough such that hydraulic conductivity drop near root surface
 440 can be resolved. The axial and radial conductances are high, such that the pressure inside the root
 441 is everywhere the same and the uptake flux is uniform.

442 **Required output** The following simulation results of participating models are to be uploaded
 443 via pull requests to this path on the github repository: M3 Water flow in roots/M3.2 Root
 444 system/M32a Numerical results and M3 Water flow in roots/M3.2 Root system/M32b Numerical
 445 results for the constant and age-dependent root hydraulic properties cases.

Figure 9: Results of C1.1: Soil water pressure head gradients around a single, transpiring, root at the onset of stress and the time of its occurrence



446 1. A text file consisting of two rows containing comma separated radial distances from the
 447 root surface (cm) in the first, and soil pressure head (cm) in the second for each soil and
 448 transpiration rate scenario (i.e., 3 (soils) \times 2 (transpiration rates) \times 2 = 12 rows. The file
 449 name should be of the form "simulatorname.txt", e.g. "DuMux.txt".

450 Note that we do not prescribe spatial or temporal resolution of the outputs, as that may depend
 451 on the individual numerical schemes.

452 2.1.5 C1.2: Water uptake by a root system from drying soil

This benchmark scenario considers water uptake by a static 8-day-old lupine root system given in the public data set (Koch, 2019) as RSML or DGF. The root is the same as the one in benchmark M3.2, only younger, in order to reduce the computational cost for the reference scenario. The root system has been segmented from MRI measurements. The lupine is embedded in a soil box of $l \times w \times d = 8 \times 8 \times 15 \text{ cm}$ filled with loam (soil hydraulic properties given in Table 3). The benchmark is to evaluate the accuracy of root water uptake models under conditions of drying soil. To this end, the soil has an initial water content of $\theta_{top} = 0.129$, corresponding to a pressure head $\psi_{s,top} = -659.8 \text{ cm}$ at the soil surface ($z = 0$). The pressure head in the rest of the domain

initially follows a hydrostatic distribution

$$\psi_{s,i} = \psi_{s,\text{top}} - z, \quad (14)$$

where z (in cm) denotes the vertical position (upward-pointing axis, zero at soil surface). At all soil boundaries, as well as at the root tips, no-flux boundaries are prescribed. A potential transpiration rate is given as the sinusoidal diurnal function

$$Q_{\text{pot}}(t) = \bar{Q} \left[1 + \sin \left(2\pi t - \frac{\pi}{2} \right) \right], \quad (15)$$

453 where the mean transpiration rate is $\bar{Q} = 6.4 \text{ cm}^3 \text{ d}^{-1}$, the time t is given in days, and $Q_{\text{pot}}(t =$
 454 $0) = 0$, that is, the simulation starts at night. The potential transpiration rate Q_{pot} , Eq. (15),
 455 is enforced at the root collar (Neumann boundary condition) as long as the root water pressure
 456 head at the root collar is above $\psi_{x,\text{crit}} = -15.290 \text{ cm}$ (corresponding to -1.5 MPa). If this critical
 457 root water pressure head at the root collar is reached, the boundary condition is switched to a
 458 Dirichlet type boundary condition, enforcing a constant pressure head $\psi_{x,\text{crit}} = -15.290 \text{ cm}$ at
 459 the root collar. This informal description is intentional, as the actual implementation of such a
 460 boundary condition may vary from simulator to simulator. We consider two scenarios. In scenario
 461 C1.2a the root hydraulic properties are constant. The tap root and lateral root conductivities
 462 are $k_x = 4.32 \times 10^{-2} \text{ cm}^3 \text{ d}^{-1}$ and $k_r = 1.73 \times 10^{-4} \text{ d}^{-1}$ (Table 4). For scenario C1.2b the root
 463 hydraulic properties depend on the root type and root age and are shown in Fig. 7.

Given the soil domain Ω and the network of root center-lines Λ , we solve the following coupled system of equations

$$\frac{\partial \theta}{\partial t} - \nabla \cdot (K(\theta)(\nabla \psi_s + e_3)) = q(\psi_x, \psi_s) \quad \text{in } \Omega, \quad (16)$$

$$-\frac{\partial}{\partial \zeta} \left(k_x \frac{\partial \psi_x}{\partial \zeta} + \frac{\partial z}{\partial \zeta} \right) = \hat{q}(\psi_x, \psi_s) \quad \text{on } \Lambda, \quad (17)$$

464 subject to the boundary conditions specified above, where ζ is a scalar parametrisation (local axial
 465 coordinate) of the root segments. The specific radial flux \hat{q} in units ($\text{cm}^2 \text{ d}^{-1}$) is given by the average
 466 soil water pressure head on the root surface. The formulation of q in Eq. (16) may be different
 467 between different participating models. A discussion on singularity issues when evaluating the soil
 468 water content at the root center line can be found in Koch et al. (2018b). In many cases, the soil
 469 discretisation is much larger than the root diameter, and thus the drop in hydraulic conductivity
 470 near the root surface in dry soils may not be sufficiently resolved in the soil domain. Approaches to
 471 estimate soil water pressure head drop at the root-soil interface from bulk soil values can be found
 472 in Mai et al. (e.g. 2019); Beudez et al. (e.g. 2013). Different approaches for the determination of
 473 the sink term for root water uptake are likely to differ most in dry soil. The reference solution to
 474 this benchmark is designed to evaluate possible differences between the models in that regard.

Reference solution As no analytical solutions exist for this problem of coupled water flow in the soil-root system, we designed a reference solution with a numerical model that explicitly considers the physical presence of roots in the soil domain, i.e., the soil mesh is highly refined around all roots and water uptake is modelled via boundary conditions at all the root surfaces. Thus, this reference solution does not make any assumptions that are inherent in the definition of the sink terms for root water uptake in the line source-based models. An explicit 3D soil grid is also used in Daly et al. (2017). However here, the soil is additionally coupled to the xylem flow in the root. The root is still modeled as a network of one-dimensional segments (center-line representation). Each segment has a specific radius as specified in the RSML grid file to this benchmark. A three-dimensional representation of the root system is implicitly given by the union of all spheres along the root center-lines. Using this implicit representation a soil grid excluding the root system was generated using the C++ geometry library CGAL (The CGAL Project, 2019). In order to reduce the number of vertices in the mesh, the mesh is locally refined around the root-soil interface. The resulting mesh is available in the Gmsh format (Geuzaine and Remacle, 2009) in the data set. For the evaluation of the radial flux, which is a coupling condition on the soil faces σ representing the root-soil interface, we integrate over each face

$$F_r = \int_{\sigma} r_{\text{root}} k_r (\psi_s - \psi_x) dA. \quad (18)$$

475 While the soil water pressure head is defined on the face, the corresponding root xylem water
476 pressure head has to be found by a mapping. To this end the integration point is first mapped onto
477 the root surface using its implicit representation. Then the point is mapped onto the corresponding
478 root center-line (a line segment) by finding the closest point on the line segment. There, ψ_x is
479 evaluated. The flux is added as a source term in the corresponding segment in the root. The
480 model is implemented in the open-source porous media simulator DuMu^x (Flemisch et al., 2011;
481 Koch et al., 2019; Koch et al., 2018a). The coupled system is solved with a fully coupled manner,
482 using Newton's method, and monolithic linear solver (block-preconditioned stabilized bi-conjugate
483 gradient solver) in each Newton iteration. The equations are discretized in time with an implicit
484 Euler method, and in space with a locally mass conservative vertex-centered finite volume method
485 (BOX method (Helmig et al., 1997)). The maximum time step size is $\Delta t = 1200$ s. The actual time
486 step size may be sometimes chosen smaller, depending on the convergence speed of the Newton
487 method. Output files are produced in regular intervals every 1200 s starting with the initial solution.
488 The simulation time is 3 d.

489 Soil water content and root water pressure head in a three-dimensional plot is shown in Fig.
490 10 for C1.2b. Fig. 11A shows the potential and actual transpiration rates for both scenarios,
491 with constant and age-dependent root hydraulic properties. The curves hardly differ since the
492 water pressure head drop is dominated by the low conductivity of the dry soil. In Fig. 11B, the
493 differences between scenarios are more clearly visible in terms of the minimal and maximal root
water pressure head with respect to time.

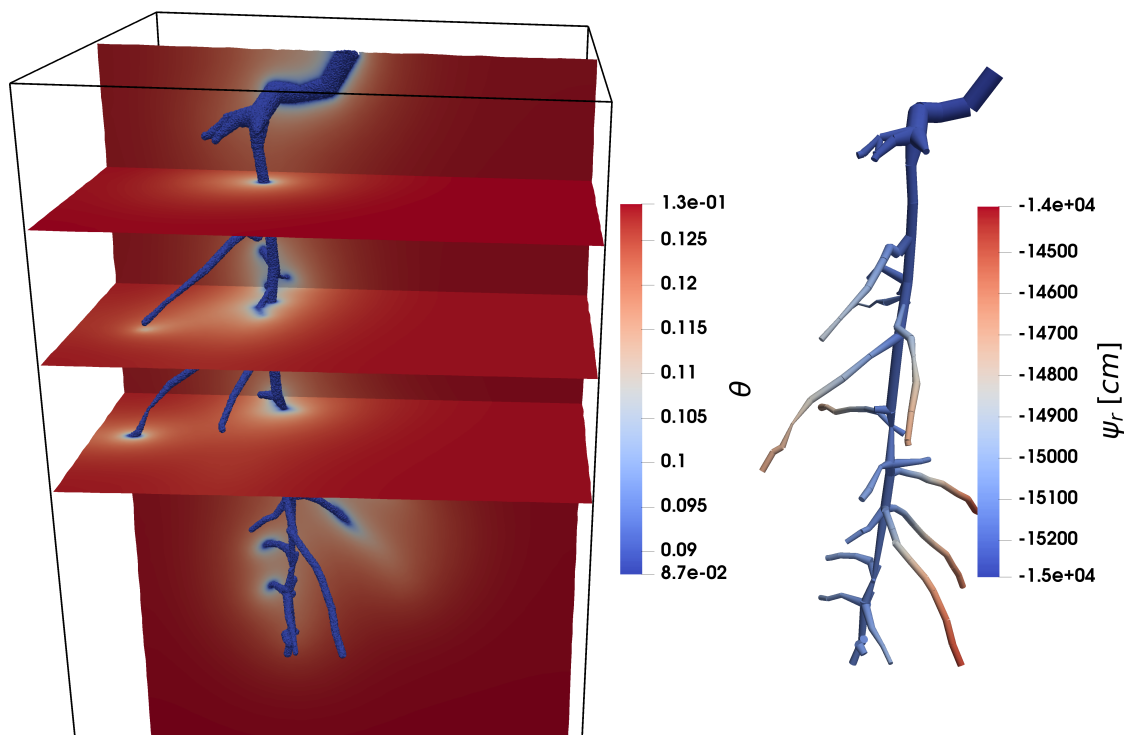


Figure 10: C1.2: Root water uptake by a static root system over time. Soil colours denote volumetric water content, root colours denote root water pressure head.

494

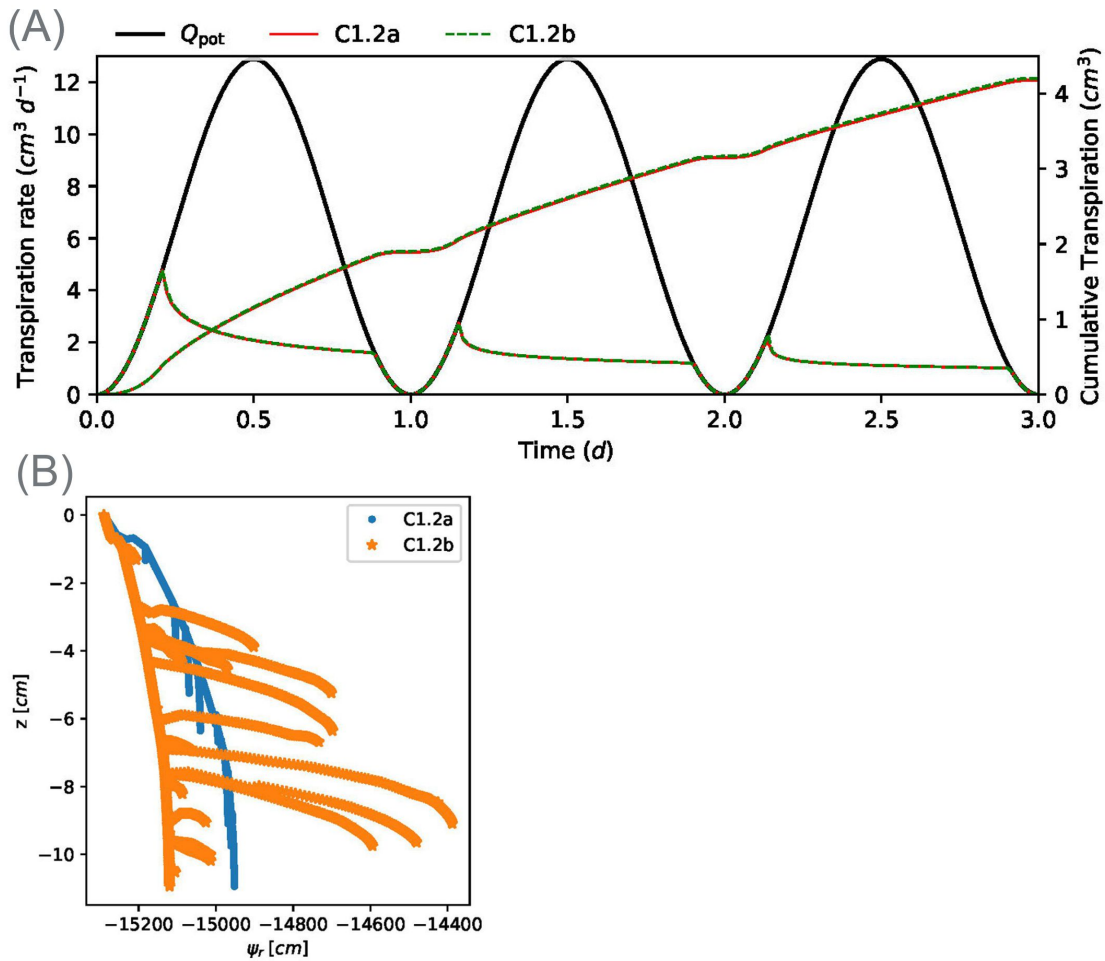


Figure 11: Results of C1.2 for two scenarios, constant and age-dependent root hydraulic properties. A: Actual transpiration of reference solution. B: Root water pressure head distributions inside the root system.

495 **Required outputs** To compare the results between the participating models, the desired
 496 outputs are

- 497 • VTK files (3D) of soil water pressure head and water content on the first, second and third
 498 day ($t = 0.5$ d, 1.5 d, 2.5 d). For output written every 1200s this means the output files with
 499 the number 36, 108, and 180.
- 500 • VTK files (lines in 3D) of root water pressure head in the first, second and day ($t =$
 501 0.5 d, 1.5 d, 2.5 d)
- 502 • CSV file with three data points per time step (each 1200s starting with $t = 0$): time and
 503 actual transpiration rate
- 504 • CSV file with three data point per time step: time and minimum and maximum root water
 505 pressure head

506 File names of the VTK files should indicate the simulator name, the state variable, the domain, and
 507 the output time in days, e.g. "DuMux_soil_theta_1d.vtk". File names of the CSV files should
 508 indicate the simulator name and output time it days, e.g., "Dumux_1.csv".

509 2.2 Coupled benchmark scenarios C2: Root water uptake by a dynamic 510 root system

511 In this benchmark, we wish to explore differences caused by the approach of root growth modelling.
512 We assess how the differences in root architecture parameters resulting from M1.2 propagate (or
513 not) in the computation of the root water uptake from soil. In this example, we do not consider
514 the effect of soil properties on root growth, but only the differences that arise from the different
515 root systems according to M1.2.

516 2.2.1 C2.1: Water uptake by a single root

517 Before looking at the root system, we look at how the implementation of the growth itself affects
518 computed root water uptake for a single root. This scenario is analogous to C1.1, but with a single
519 root growing at an elongation rate of 2 cm/d from 1 to 10 cm length.

520 **Required outputs** The required outputs for model intercomparison are

- 521 • VTK files of 3D soil water pressure head and water content in soil at a temporal resolution
522 of 1 day up until 60 days (point data)
- 523 • VTK files of xylem water pressure head (point data)
- 524 • Text files with two lines: time and corresponding actual transpiration

525 2.2.2 C2.2: Water uptake by a root system

526 This scenario is the same as C1.2b, but replacing the static root system with a growing root
527 system. The root growth parameters are for each model the results of M1.2; simulations start from
528 a seed and run until a 60 day old root system. The domain size is $25 \times 25 \times 100$ cm, the potential
529 transpiration $Q_{pot} = 0.5 \text{ cm}^3 \text{ d}^{-1}$ is scaled proportional to the root volume divided by the maximal
530 root volume at maturity.

531 **Required outputs**

- 532 • VTK files of 3D soil water pressure head and water content in soil at a temporal resolution
533 of 1 day up until 60 days (point data)
- 534 • VTK files of xylem water pressure head (point data)
- 535 • Text files with two lines: time and corresponding actual transpiration

536 File names of the VTK files should indicate the simulator name, the state variable, the domain, and
537 the output time in days, e.g. "DuMux_soil_theta_1d.vtk". File names of the CSV files should
538 indicate the simulator name and output time in days, e.g., "Dumux_1.csv".

539 2.3 Automated comparison within all benchmark problems

540 Each benchmark folder on the github repository contains a Jupyter Notebook named "Automated
541 comparison". It provides the analytical solution of the respective benchmark and in addition
542 includes Python code that automatically loads all the outputs of participating models that are
543 provided in the "Numerical results" folder of that benchmark. As soon as new outputs are provided,
544 they are automatically included in the analysis. Currently, different model outputs are already
545 available. We envision more participating models' outputs to be provided in this way. Future
546 analysis will include graphical and quantitative approaches.

547 3 Conclusions

548 Functional-structural root architecture models have been compared qualitatively (Dunbabin et al.,
549 2013, e.g.), but until now no quantitative benchmarking existed. In other communities, bench-
550 marking has been done or is ongoing, e.g., AgMIP (Porter et al., 2014) for crop models, CMIP
551 (Eyring et al., 2016) for climate models, subsurface reactive transport models (Steeffel et al., 2015).

552 With this paper, we propose a framework for collaborative benchmarking of functional-structural
553 root architecture models that allows quantitative comparison of the outputs of different simulators
554 with reference solutions and with each other. This framework is presented using Jupyter Note-
555 books. Behind every "module" benchmark, there is a working code that explains and implements
556 the reference solution or analysis of reference data. For both, "module" and "coupled" benchmarks,
557 Jupyter Notebooks facilitate the automated comparison of simulator simulation outputs that are
558 stored in specified folders of a public github repository. In this way, new numerical simulators
559 that may be developed in the future may still be added to the automated comparison. All the
560 analysis that is done in the Jupyter Notebooks is freely available so that the comparisons and
561 analysis of uploaded model outputs will be transparent and repeatable. Future efforts will aim at
562 extending the benchmarks from water flow in root and soil systems to further processes such as
563 solute transport, rhizodeposition, etc. We expect that this benchmarking will result in a better
564 understanding of the different models and contribute towards improved models, with which we can
565 simulate various scenarios with greater confidence. It will set standards for future model devel-
566 opments, ensuring that bugs, numerical errors or conceptual misunderstandings do not affect the
567 value of future work. This is a step towards developing those models into the much-needed aid
568 in the design of agricultural management schemes and model-guided crop breeding. These models
569 may also be useful in ecology, e.g. to study species complementarity.

570 Acknowledgements

571 A.S. acknowledges funding by the German Research Foundation (grant number SCHN 1361/3-1).
572 V.C. was supported by the Belgian Fonds National de la Recherche Scientifique (FNRS, grant
573 FC84104). V.S. acknowledges funding by the German Research Foundation (grant number SCHM
574 997/33-1). This research was institutionally funded by the Helmholtz Association (POF III Pro-
575 gram—Research Fields Key Technologies for the Bioeconomy and Terrestrial Environment).

576 References

- 577 Simulating the role of rooting traits in crop-weed competition. *Field Crops Research*, 104:44–51.
- 578 Anderson, M. J. (2001). A new method for non-parametric multivariate analysis of variance.
579 *Australian Journal of Ecology*, 26:32–46.
- 580 Bastian, P., Blatt, M., Dedner, A., Engwer, C., Klöfkorn, R., Ohlberger, M., and Sander, O.
581 (2008). A generic grid interface for parallel and adaptive scientific computing. part I: Abstract
582 framework. *Computing*, 82(2–3):103–119.
- 583 Beudez, N., Doussan, C., Lefeuvre-Mesgouez, G., and Mesgouez, A. (2013). Influence of three root
584 spatial arrangement on soil water flow and uptake. results from an explicit and an equivalent,
585 upscaled, model. *Procedia Environmental Sciences*, 19:37–46.
- 586 Bidel, L. P. R., Pagès, L., Rivière, L. M., Pelloux, G., and Lorendeau, J. Y. (2000). MassFlowDyn
587 I: A carbon transport and partitioning model for root system architecture. *Annals of Botany*,
588 85(6):869–886.
- 589 Daly, K. R., Tracy, S. R., Crout, N. M., Mairhofer, S., Pridmore, T. P., Mooney, S. J., and Roose,
590 T. (2017). Quantification of root water uptake in soil using X-ray computed tomography and
591 image-based modelling. *Plant, Cell & Environment*, 41:121–133.
- 592 Delory, B. B. M., Li, M., Topp, C. C. N., and Lobet, G. (2018). archiDART v3.0: A new data
593 analysis pipeline allowing the topological analysis of plant root systems. *F1000Research*, 7:22.
- 594 Delory, B. M., Baudson, C., Brostaux, Y., Lobet, G., du Jardin, P., Pagès, L., and Delaplace, P.
595 (2016). archiDART: An R package for the automated computation of plant root architectural
596 traits. *Plant and Soil*, 398(1):351–365.
- 597 Doussan, C., Pagès, L., and Vercambre, G. (1998). Modelling of the hydraulic architecture of root
598 systems: An integrated approach to water absorption—model description. *Annals of Botany*,
599 81(2):213–223.
- 600 Dunbabin, V. M., McDermott, S., and Bengough, A. G. (2006). Upscaling from rhizosphere to
601 whole root system: Modelling the effects of phospholipid surfactants on water and nutrient
602 uptake. *Plant and Soil*, 283:57–72.
- 603 Dunbabin, V. M., Postma, J. A., Schnepf, A., Pagès, L., Javaux, M., Wu, L., Leitner, D.,
604 Chen, Y. L., Rengel, Z., and Diggle, A. J. (2013). Modelling root-soil interactions using three-
605 dimensional models of root growth, architecture and function. *Plant and Soil*, 372(1/2):93–124.
- 606 Dupuy, L. X., Fourcaud, T., Lac, P., and Stokes, A. (2007). A generic 3D finite element model of
607 tree anchorage integrating soil mechanics and real root system architecture. *American Journal*
608 *of Botany*, 94:1506–1514.
- 609 Eyring, V., Bony, S., Meehl, G. A., Senior, C. A., Stevens, B., Stouffer, R. J., and Taylor, K. E.
610 (2016). Overview of the coupled model intercomparison project phase 6 (CMIP6) experimental
611 design and organization. *Geoscientific Model Development*, 9(5):1937–1958.
- 612 Fitter, A. H. (1987). An architectural approach to the comparative ecology of plant root systems.
613 *New Phytologist*, 106(s1):61–77.
- 614 Fitter, A. H. and Stickland, T. R. (1991). Architectural analysis of plant root systems 2. Influence
615 of nutrient supply on architecture in contrasting plant species. *New Phytologist*, 118(3):383–389.

- 616 Flemisch, B., Darcis, M., Erbertseder, K., Faigle, B., Lauser, A., Mosthaf, K., Müthing, S., Nuske,
617 P., Tatomir, A., Wolff, M., and Helmig, R. (2011). DuMu^x: DUNE for multi-{phase, component,
618 scale, physics,...} flow and transport in porous media. *Advances in Water Resources*, 34(9):1102–
619 1112.
- 620 Geuzaine, C. and Remacle, J.-F. (2009). Gmsh: A 3-D finite element mesh generator with built-in
621 pre- and post-processing facilities. *International Journal for Numerical Methods in Engineering*,
622 79(11):1309–1331.
- 623 Helmig, R. et al. (1997). *Multiphase Flow and Transport Processes in the Subsurface: A Contri-*
624 *bution to the Modeling of Hydrosystems*. Springer-Verlag.
- 625 Hund, A., Trachsel, S., and Stamp, P. (2009). Growth of axile and lateral roots of maize: I
626 development of a phenotyping platform. *Plant and Soil*, 325(1):335–349.
- 627 Janssen, P. and Heuberger, P. (1995). Calibration of process-oriented models. *Ecological Modelling*,
628 83(1):55–66. Modelling Water, Carbon and Nutrient Cycles in Forests.
- 629 Javaux, M., Schröder, T., Vanderborght, J., and Vereecken, H. (2008). Use of a three-dimensional
630 detailed modeling approach for predicting root water uptake. *Vadose Zone Journal*, 7(3):1079–
631 1088.
- 632 Koch, T. (2019). Benchmark C1.2 - Numerical results reference solution. doi:10.18419/darus-471.
- 633 Koch, T., Gläser, D., Weishaupt, K., Ackermann, S., Beck, M., Becker, B., Burbulla, S., Class,
634 H., Coltman, E., Emmert, S., Fetzer, T., Grüninger, C., Heck, K., Hommel, J., Kurz, T., Lipp,
635 M., Mohammadi, F., Scherrer, S., Schneider, M., Seitz, G., Stadler, L., Utz, M., Weinhardt, F.,
636 and Flemisch, B. (2019). DuMu^x 3 – an open-source simulator for solving flow and transport
637 problems in porous media with a focus on model coupling. *arXiv e-prints*, page arXiv:1909.05052.
- 638 Koch, T., Gläser, D., Weishaupt, K., Ackermann, S., Beck, M., Becker, B., Burbulla, S., Class, H.,
639 Coltman, E., Fetzer, T., Flemisch, B., Grüninger, C., Heck, K., Hommel, J., Kurz, T., Lipp, M.,
640 Mohammadi, F., Schneider, M., Seitz, G., Scholz, S., and Weinhardt, F. (2018a). Dumux 3.0.0.
- 641 Koch, T., Heck, K., Schröder, N., Class, H., and Helmig, R. (2018b). A new simulation framework
642 for soil-root interaction, evaporation, root growth, and solute transport. *Vadose Zone Journal*,
643 17.
- 644 Landl, M., Schnepf, A., Vanderborght, J., Bengough, A. G., Bauke, S. L., Lobet, G., Bol, R., and
645 Vereecken, H. (2018). Measuring root system traits of wheat in 2d images to parameterize 3d
646 root architecture models. *Plant and Soil*, 425(1):457–477.
- 647 Landsberg, J. and Fowkes, N. (1978). Water movement through plant roots. *Annals of Botany*,
648 42(3):493–508.
- 649 Li, M., Duncan, K., Topp, C. N., and Chitwood, D. H. (2017). Persistent homology and the
650 branching topologies of plants. *American Journal of Botany*, 104(3):1–5.
- 651 Li, M., Frank, M. H., Coneva, V., Mio, W., Chitwood, D. H., and Topp, C. N. (2018). The persistent
652 homology mathematical framework provides enhanced genotype-to-phenotype associations for
653 plant morphology. *Plant Physiology*, 177:1382–1395.
- 654 Lobet, G., Pagès, L., and Draye, X. (2011). A novel image-analysis toolbox enabling quantitative
655 analysis of root system architecture. *Plant Physiology*, 157:29–39.
- 656 Lobet, G., Pound, M. P., Diener, J., Pradal, C., Draye, X., Godin, C., Javaux, M., Leitner, D.,
657 Meunier, F., Nacry, P., Pridmore, T. P., and Schnepf, A. (2015). Root System Markup Language:
658 Toward a unified root architecture description language. *Plant Physiology*, 167:617–627.
- 659 Luo, Y. Q., Randerson, J. T., Abramowitz, G., Bacour, C., Blyth, E., Carvalhais, N., Ciais,
660 P., Dalmonech, D., Fisher, J. B., Fisher, R., Friedlingstein, P., Hibbard, K., Hoffman, F.,
661 Huntzinger, D., Jones, C. D., Koven, C., Lawrence, D., Li, D. J., Mahecha, M., Niu, S. L.,
662 Norby, R., Piao, S. L., Qi, X., Peylin, P., Prentice, I. C., Riley, W., Reichstein, M., Schwalm,
663 C., Wang, Y. P., Xia, J. Y., Zaehle, S., and Zhou, X. H. (2012). A framework for benchmarking
664 land models. *Biogeosciences*, 9:3857–3874.

- 665 Mai, T. H., Schnepf, A., Vereecken, H., and Vanderborght, J. (2019). Continuum multiscale model
666 of root water and nutrient uptake from soil with explicit consideration of the 3D root architecture
667 and the rhizosphere gradients. *Plant and Soil*, 439:273–292.
- 668 Meunier, F., Draye, X., Vanderborght, J., Javaux, M., and Couvreur, V. (2017). A hybrid
669 analytical-numerical method for solving water flow equations in root hydraulic architectures.
670 *Applied Mathematical Modelling*, 52:648–663.
- 671 Nygren, P. and Perttunen, J. (2010). Rhizodeposition: a carbon efflux often neglected in functional-
672 structural plant models. In *Proceedings of the 6th International Workshop on Functional-
673 Structural Plant Models*.
- 674 Oram, N. J., Ravenek, J. M., Barry, K., Weigelt, A., Chen, H., Gessler, A., Gockele, A., de Kroon,
675 H., van der Paauw, J. W., Scherer-Lorenzen, M., Smit-Tiekstra, A., van Ruijven, J., and Mom-
676 mer, L. (2018). Below-ground complementarity effects in a grassland biodiversity experiment
677 are related to deep-rooting species. *Journal of Ecology*, 106:265–277.
- 678 Porter, C. H., Villalobos, C., Holzworth, D., Nelson, R., White, J. W., Athanasiadis, I. N., Janssen,
679 S., Ripoche, D., Cufi, J., Raes, D., Zhang, M., Knapen, R., Sahajpal, R., Boote, K., and Jones,
680 J. W. (2014). Harmonization and translation of crop modeling data to ensure interoperability.
681 *Environmental Modelling & Software*, 62:495–508.
- 682 Roose, T. and Fowler, A. (2004). A model for water uptake by plant roots. *Journal of Theoretical
683 Biology*, 228(2):155–171.
- 684 Schnepf, A., Huber, K., Landl, M., Meunier, F., Petrich, L., and Schmidt, V. (2018). Statistical
685 characterization of the root system architecture model CRootBox. *Vadose Zone Journal*, 17(1).
- 686 Schröder, T., Javaux, M., Vanderborght, J., Körfgen, B., and Vereecken, H. (2008). Effect of local
687 soil hydraulic conductivity drop using a three-dimensional root water uptake model. *Vadose
688 Zone Journal*, 7.
- 689 Schroeder, W., Martin, K., and Lorensen, B. (2006). *The Visualization Toolkit*. Kitware, 4th
690 edition.
- 691 Steefel, C. I., Yabusaki, S. B., and Mayer, K. U. (2015). Reactive transport benchmarks for
692 subsurface environmental simulation. *Computational Geosciences*, 19(3):439–443.
- 693 The CGAL Project (2019). *CGAL User and Reference Manual*. CGAL Editorial Board, 4.14
694 edition.
- 695 Van Genuchten, M. (1980). Closed-form equation for predicting the hydraulic conductivity of
696 unsaturated soils. *Soil Science Society of America Journal*, 44(5):892–898.
- 697 Vanderborght, J., Kasteel, R., Herbst, M., Javaux, M., Thiéry, D., Vanclooster, M., Mouvet, C.,
698 and Vereecken, H. (2005). A set of analytical benchmarks to test numerical models of flow and
699 transport in soils. *Vadose Zone Journal*, 4(1):206–221.
- 700 Zarebanadkouki, M., Meunier, F., Couvreur, V., Cesar, J., Javaux, M., and Carminati, A. (2016).
701 Estimation of the hydraulic conductivities of lupine roots by inverse modelling of high-resolution
702 measurements of root water uptake. *Annals of Botany*, 118(4):853–864.

703 A Derivation of the analytical solution of water flow inside 704 the root system

705 The axial water flow rate in the xylem Q_x ($\text{cm}^3 \text{ day}^{-1}$) is given by

$$Q_x = -k_x \left(\frac{\partial \psi_x}{\partial \zeta} + v \cdot \mathbf{e}_3 \right), \quad (19)$$

706 where k_x is the axial conductance ($\text{cm}^3 \text{ day}^{-1}$), ψ_x is the pressure inside the xylem (cm), ζ is
707 the local axial coordinate \mathbf{e}_3 the unit vector in z -direction, and v the normalised direction of the
708 xylem.

709 The radial water flow rate is given by

$$Q_r = -2r_{root}\pi l_{seg}k_r(\psi_s - \psi_x) \quad (20)$$

710 with units ($\text{cm}^3 \text{ day}^{-1}$), where r_{root} is the root radius (cm), l_{seg} is the length of each root segment
 711 (cm), k_r is the radial conductivity (day^{-1}), and ψ_s is the soil water pressure head of the surround-
 712 ing soil (cm). The equation is neglecting osmotic potential and is based on Eq. (3.3) of Roose
 713 and Fowler (2004). Note that around the root a homogeneous soil water pressure head is assumed,
 714 therefore there is actually no hydrostatic equilibrium.

715

For each segment of length l_{seg} mass conservation yields

$$0 = Q_x|_{l_{seg}} - Q_x|_0 + Q_r \quad (21)$$

$$-\frac{1}{l_{seg}}Q_r = -\frac{1}{l_{seg}}(Q_x|_0 - Q_x|_{l_{seg}}) \quad \text{and for } l_{seg} \rightarrow 0 \quad (22)$$

$$2r_{root}\pi k_r(\psi_s - \psi_x) = -k_x \frac{\partial^2 \psi_x}{\partial \zeta^2} \quad (23)$$

716 see Eq. (3.4) of Roose and Fowler (2004), where v_3 is the z -component of the normalised xylem
 717 direction (cm).

Integrating this ordinary differential equation leads to an explicit equation for $\psi_x(\zeta)$

$$\psi_x(\zeta) = \psi_s + d_1 e^{\sqrt{c}\zeta} + d_2 e^{-\sqrt{c}\zeta}, \quad (24)$$

718 where $c := 2a\pi k_r/k_x$, and d_1 , and d_2 are integration constants that are derived from the boundary
 719 conditions.

720

721 To exemplify, we calculate d_1 , and d_2 for a Dirichlet boundary condition at the root collar, and
 722 no-flux boundary conditions at the tip. The Dirichlet boundary conditions at the collar of the root
 723 system $\psi_x|_{\text{collar}} = \psi_0$ is inserted into the analytic solution Eq. (24), and yields

$$\psi_s + d_1 + d_2 = \psi_0. \quad (25)$$

724 The Neumann boundary condition $Q_x|_{l_{seg}} = 0$ (Eq. 20) leads to

$$\frac{\partial \psi_x}{\partial \zeta}|_{l_{seg}} = v_3, \quad (26)$$

725 where l_{seg} is the length of the root segment. Using the derivation of the analytical solution yields

$$d_1 \sqrt{c} e^{\sqrt{c}l_{seg}} - d_2 \sqrt{c} e^{-\sqrt{c}l_{seg}} = v_3. \quad (27)$$

For a straight downward segment $v_3 = -1$, Eqns (25) and (27) can be summarized as

$$\begin{pmatrix} 1 & 1 \\ \sqrt{c}e^{\sqrt{c}l_{seg}} & -\sqrt{c}e^{-\sqrt{c}l_{seg}} \end{pmatrix} \begin{pmatrix} d_1 \\ d_2 \end{pmatrix} = \begin{pmatrix} \psi_0 - \psi_s \\ -1 \end{pmatrix} \quad (28)$$

Solving this linear equation for d_1 and d_2 yields

$$d_1 = d^{-1} \left(e^{-\sqrt{c}l_{seg}} (\psi_0 - \psi_s) + 1 \right) \quad (29)$$

$$d_2 = -d^{-1} \left(e^{\sqrt{c}l_{seg}} (\psi_0 - \psi_s) + 1 \right), \quad (30)$$

where d is the determinant of above matrix

$$d = e^{-\sqrt{c}l_{seg}} - e^{\sqrt{c}l_{seg}}. \quad (31)$$